Updated on 28 Feb 2013

EFFECT OF PYRIDOXAL PHOSPHATE AND TETRAHYDROFOLATE BOUND ON HUMAN SERINE HYDROXYMETHYLTRANSFERASE BY MOLECULAR DYNAMIC SIMULATION

Mr. Peerapong Wongpituk

จุฬาลงกรณ์มหาวิทยาลัย
CHULALONGKORN UNIVERSITY

A Thesis Submitted in Partial Fulfillment of the Requirements
for the Degree of Master of Science in Chemistry
Department of Chemistry
FACULTY OF SCIENCE
Chulalongkorn University
Academic Year 2020

Copyright of Chulalongkorn University

Updated on 28 Feb 2013

ผลของไพริดอกซอลฟอสเฟตและเททระไฮโดรโฟเลตที่ยึดจับกับเซอรีนไฮดรอกซีเมทิลแทรนส์เฟอเรสของมนุษย์โดยการจำลองพลวัตเชิงโมเลกุล

นายพีรพงศ์ วงศ์พิทักษ์

จุฬาลงกรณ์มหาวิทยาลัย
CHULALONGKORN UNIVERSITY

วิทยานิพนธ์นี้เป็นส่วนหนึ่งของการศึกษาตามหลักสูตรปริญญาวิทยาศาสตรมหาบัณฑิต
สาขาวิชาเคมี ภาควิชาเคมี
คณะวิทยาศาสตร์ จุฬาลงกรณ์มหาวิทยาลัย
ปีการศึกษา 2563
ลิขสิทธิ์ของจุฬาลงกรณ์มหาวิทยาลัย

Thesis Title	EFFECT OF PYRIDOXAL PHOSPHATE AND TETRAHYDROFOLATE BOUND ON HUMAN SERINE HYDROXYMETHYLTRANSFERASE BY MOLECULAR DYNAMIC SIMULATION
By	Mr. Peerapong Wongpituk
Field of Study	Chemistry
Thesis Advisor	Professor SUPOT HANNONGBUA, Ph.D.
Thesis Co Advisor	Assistant Professor THANYADA RUNGROTMONGKOL, Ph.D.

Accepted by the FACULTY OF SCIENCE, Chulalongkorn University in Partial Fulfillment of the Requirement for the Master of Science

..... Dean of the FACULTY OF SCIENCE
(Professor POLKIT SANGVANICH, Ph.D.)

THESIS COMMITTEE

..... Chairman
(Professor VUDHICHAI PARASUK, Ph.D.)

..... Thesis Advisor
(Professor SUPOT HANNONGBUA, Ph.D.)

..... Thesis Co-Advisor
(Assistant Professor THANYADA RUNGROTMONGKOL, Ph.D.)

..... Examiner
(Associate Professor SOMSAK PIANWANIT, Ph.D.)

..... External Examiner
(Penchit Chitnumsub, Ph.D.)

จุฬาลงกรณ์มหาวิทยาลัย
Chulalongkorn University

พีรพงศ์ วงศ์พิทักษ์ : ผลของไพริดอกซอลฟอสเฟตและเททระไฮโดรโฟเลตที่ยึดจับกับเซอรีนไฮดรอกซีเมทิลแทรนส์เฟอเรสของมนุษย์โดยการจำลองพลวัตเชิงโมเลกุล. (EFFECT OF PYRIDOXAL PHOSPHATE AND TETRAHYDROFOLATE BOUND ON HUMAN SERINE HYDROXYMETHYLTRANSFERASE BY MOLECULAR DYNAMIC SIMULATION) อ.ที่ปรึกษาหลัก : ศ. ดร.สุพจน์ หารหนองบัว, อ.ที่ปรึกษาร่วม : ผศ. ดร. ธัญญดา รุ่งโรจน์มงคล

เซอรีนไฮดรอกซีเมททิลทรานเฟอร์เรส เป็นเอนไซม์ที่ทำงานร่วมกับไพริดอกซัลฟอสเฟตในกระบวนการเมแทบอลิซึมของคาร์บอนหนึ่งหน่วย ซึ่งเกี่ยวข้องกับหลายกระบวนทางชีวเคมี รวมถึงการสังเคราะห์ทางชีวเคมีของพิวรีนและไทมิดีน เอนไซม์ชนิดนี้ของมนุษย์ โดยเฉพาะเซอรีนไฮดรอกซีเมททิลทรานเฟอร์เรส 1 ถูกศึกษาอย่างแพร่หลาย เพื่อใช้เป็นเป้าหมายในการพัฒนายาเคมีบำบัดสำหรับรักษาโรคมะเร็ง ด้วยเหตุนี้ กระบวนการทำงานของเอนไซม์ชนิดนี้จึงมีความสำคัญ ดังนั้นในงานวิจัยนี้มีเป้าหมายเพื่อศึกษากลไกการเกิดปฏิกิริยาทางเคมีและศึกษาลักษณะการยึดจับกับลิแกนด์ต่าง ๆ ด้วยการจำลองพลวัติเชิงโมเลกุลของเอนไซม์เซอรีนไฮดรอกซีเมททิลทรานเฟอร์เรส 1 ในมนุษย์ รูปแบบเตตระเมอร์ เป็นเวลา 500 นาโนวินาที ทั้งหมด 6 ระบบ ตามลิแกนด์ที่แตกต่างกัน (PLP-Lys, L-ser, PLS, PLG, THF และ MTHF) พบว่ามีกรดอะมิโนที่สำคัญดังนี้ Y’73, S53, H231, K257, R263 และ Y402 เกิดพันธะกับลิแกนด์ในทุกระบบอย่างมีนัยสำคัญ ขณะเดียวกัน กรดอะมิโน S119 และ G120 เกิดพันธะไฮโดรเจนแบบแข็งแกร่งกับลิแกนด์ในทุกระบบ นอกจากนี้พบว่า PLS และ PLG ส่งผลให้ระบบเกิดความเสถียรมากกว่า THF และ MTHF และระบบที่ 5 เอนไซม์เซอรีนไฮดรอกซีเมททิลทรานเฟอร์เรส ซึ่งจับกับ MTHF/PLG ให้พลังงานการยึดจับดีที่สุด จากผลการศึกษาเหล่านี้ สามารถใช้เป็นแนวทางเชิงทฤษฎีสำหรับการพัฒนาสารยับยั้งที่มีผลต่อเอนไซม์เซอรีนไฮดรอกซีเมททิลทรานเฟอร์เรส 1 เพื่อเป้าหมายในการยับยั้งมะเร็งต่อไป

สาขาวิชา เคมี ลายมือชื่อนิสิต .....

ปีการศึกษา 2563 ลายมือชื่อ อ.ที่ปรึกษาหลัก .....

ลายมือชื่อ อ.ที่ปรึกษาร่วม .....

6071973023 : MAJOR CHEMISTRY

KEYWORD: Serine hydroxymethyltransferase Molecular dynamics simulations pyridoxal phosphate L-serine

Peerapong Wongpituk : EFFECT OF PYRIDOXAL PHOSPHATE AND TETRAHYDROFOLATE BOUND ON HUMAN SERINE HYDROXYMETHYLTRANSFERASE BY MOLECULAR DYNAMIC SIMULATION. Advisor: Prof. SUPOT HANNONGBUA, Ph.D. Co-advisor: Asst. Prof. THANYADA RUNGROTMONGKOL, Ph.D.

Serine hydroxymethyltransferase (SHMT), a pyridoxal phosphate (PLP)-dependent enzyme, is involved in one-carbon metabolism in multiple biochemical pathways, including the biosynthesis of purine and thymidine. SHMT1 is the enzyme to be studied clinically as a target for cancer chemotherapy. Therefore, the binding mechanism of this enzyme would be investigated. In this study, molecular dynamics simulations for 500 ns was applied on SHMT1 tetramer in six systems with different ligand cofactors (PLP-Lys, L-ser, PLS, PLG, THF, and MTHF) in order to understand its structural dynamics properties. The key residues Y'73, S53, H231, K257, R263 and R402 were found in all ligand cofactor/SHMT1 systems. All ligand cofactors of each SHMT1 system were stabilized by a strong hydrogen bond with S119 and G120 residues. In addition, the PLS and PLG systems showed strong stabilization with SHMT1 rather than THF and MTHF. Among systems, the MTHF/PLG ligands in system 5 showed the highest binding affinity with SHMT1. Our results could be used as theoretical guidance for inhibitor developments toward SHMT1, which targeting anti-cancer inhibitors

จุฬาลงกรณ์มหาวิทยาลัย
Chulalongkorn University

Field of Study: Chemistry Student's Signature .....

Academic Year: 2020 Advisor's Signature .....

Co-advisor's Signature .....

ACKNOWLEDGEMENTS

I would like to express my sincere thanks to my thesis advisor, Prof. Dr. Supot Hannongbua and my thesis co-advisors, Assist. Prof. Dr. Thanyada Rungrotmongkol for invaluable help and constant encouragement throughout the course of this thesis. I also thanks to the Center of Excellent in Computational Chemistry for providing me the facilities and computing resources

In addition, I would like to thanks the 90th Anniversary of Chulalongkorn University Fund (Ratchadaphiseksomphot Endowment Fund). Additionally, i would like to thanks Faculty of Science, Chulalongkorn University and Thailand Research Fund (IRG5780008) and all members of Biosimulation laboratory, Department of Biochemistry, Faculty of Science, Chulalongkorn University.

Finally, I would like to thanks my family and my friends who always give me the power to work with this project.

Peerapong Wongpituk

จุฬาลงกรณ์มหาวิทยาลัย
CHULALONGKORN UNIVERSITY

TABLE OF CONTENTS

Page

..... iii

ABSTRACT (THAI) iii

..... iv

ABSTRACT (ENGLISH) iv

ACKNOWLEDGEMENTS v

TABLE OF CONTENTS vi

LIST OF TABLES ix

LIST OF FIGURES x

CHAPTER I 1

INTRODUCTION 1

1.1 Background and rationale 1

1.2 Literature reviews 4

1.3 Objective 9

1.4 Scope of reserch 9

1.5 Research methodology 9

1.6 Expected beneficial outcome(s) 10

CHAPTER II 11

THEORIES 11

2.1 Molecular dynamics (MD) 11

2.2 Basic Data Analysis 14

2.3 Binding free energy 15

จุฬาลงกรณ์มหาวิทยาลัย
Chulalongkorn University

- The Molecular Mechanics/Generalized Born Surface Area (MM/GBSA) 15

- Solvated interaction energy (SIE) 16

CHAPTER III 17

RESEARCH METHODOLOGY 17

3.1 Software 17

3.2 Preparations of Ligands 17

- PLP covalent bond with K257 of SHMT1. 17

- Preparations of L-ser, PLS, PLG, THF and MTHF. 17

3.3 Preparations of protein complexes 18

- Systems 20

3.4 Molecular dynamics (MD) simulations and analysis 20

CHAPTER IV 22

RESULTS AND DISCUSSION 22

4.1 System stability of simulation models 22

- Root-mean square deviation (RMSD) 22

- Number of hydrogen bond 22

- Number of contact atoms 24

- B-factor 25

- Distances between C7 atom of PLP-Lys and N atom of L-ser 26

4.2 Intermolecular interactions of protein-ligand interface 26

4.3 Ligand binding affinity 32

CHAPTER V 34

CONCLUSIONS 34

REFERENCES 36

จุฬาลงกรณ์มหาวิทยาลัย
Chulalongkorn University

VITA..... 45

จุฬาลงกรณ์มหาวิทยาลัย
Chulalongkorn University

LIST OF TABLES

Page

Table 1 Key amino acids in structural forming and function of SHMT which (') represent the residues from another chain. 5

Table 2 Solvated interaction energy for L-ser, PLS and PLG complexes. 33

Table 3 Solvated interaction energy for THF and MTHF complexes. 33

จุฬาลงกรณ์มหาวิทยาลัย
CHULALONGKORN UNIVERSITY

LIST OF FIGURES

Page

Figure 1 (a) The proposed schemes of serine hydroxymethyltransferase catalytic mechanism, which is the retro-aldol mechanism and (b) schematic overview of SHMT function, the cellular folate cycle involving SHMT, thymidylate synthase (TS), and dihydrofolate reductase (DHFR)..... 2

Figure 2 3D structure of tetrameric SHMT1 (PDB code 1BJ4) consist of a dimer (AB)–dimer (CD) association to form a native tetrameric quaternary structure [2]. The flap-connected region is located at the dimer interface (^{273}VKSVDPKTGKEIL^{285})..... 3

Figure 3 Compartmentalized One-Carbon Metabolism and Role of SHMT Cytosolic and Mitochondrial Isozymes 3

Figure 4 The crystal structure of human cytosolic serine hydroxymethyltransferase on the protein data bank (PDB code 1BJ4 [2])..... 7

Figure 5 Representative scheme of the mechanism behind the internal and external aldimine formation of SHMT enzymes and the specific α-elimination reaction 8

Figure 6 Comparison of THF binding to SHMT1/Δflap versus the wild-type enzyme.... 8

Figure 7 schematic of the molecular dynamics process [46]..... 13

Figure 8 2D structure of the internal aldimine (PLP-Lys), L-serine (L-ser), pyridoxal-5'-Phosphate+L-ser (PLS), Pyridoxal-5'-Phosphate+glycine (PLG), tetrahydrofolate (THF) and 5,10- methylenetetrahydrofolate (MTHF)..... 18

Figure 9 Structure of tetrameric SHMT1 (a) Surface representation showing vast inter-subunit interfaces within tight, vertically arranged dimers and contacts between the two dimers, where the secondary structure elements with the locations of PLP covalent bound with K257 (PLP-Lys) and L-ser are given in (b). 19

จุฬาลงกรณ์มหาวิทยาลัย
Chulalongkorn University

Figure 10 Six systems of SHMT1 from mechanism behind the internal and external aldimine formation for PLP-dependent enzymes and the specific α-elimination reaction [29]. 20

Figure 11 All-atom RMSDs of six SHMT1 complexes (black), including system1 (SHMT/PLP-Lys), system2 (SHMT/PLP-Lys/L-ser), system3 (SHMT/PLS), system4 (SHMT/PLS/THF), system5 (SHMT/PLG/MTHF) and system6 (SHMT/PLG). 22

Figure 12 Number of hydrogen bond of SHMT1 performed in different cofactors, relative to their initial structures for the six studied systems: system1 (SHMT/PLP-Lys), system2 (SHMT/PLP-Lys/L-ser), system3 (SHMT/PLS), system4 (SHMT/PLS/THF), system5 (SHMT/PLG/MTHF), system6 (SHMT/PLG) within 3.5 Å cut-off distance of ligands cofactors along the simulations of 500 ns. 23

Figure 13 Number of contact atoms between SHMT1 with PLP-Lys, L-ser, PLS, PLG, THF and MTHF bound each system within 3.5 Å cut-off distance of ligands along the simulations of 500 ns 24

Figure 14 Normalized B-factor at last 100 ns MD simulation of SHMT1 complexes 26

Figure 15 Distances between C7 atoms of PLP-Lys and N atom of L-ser along simulations 26

Figure 16 The percentage of H-bond occupation between ligand cofactors and SHMT1. The hydrogen bond strengths were divided into 3 levels including low (10-39%), moderate (40–69%), and strong (70–100%) interactions represented by the gradient of greenish, bluish and reddish grid cells, respectively (left). The per-residue energy (energy contribution cutoff ±1 kcal/mol) of SHMT1 complexes with difference cofactors. The important amino acids for ligand binding are shaded based on their decomposition energy, where the highest and lowest energies are ranging from green to red, respectively (right). 31

Figure 17 The electrostatic and van der Waals (vdW) energy contributions (energy contribution cutoff ±1 kcal/mol) of SHMT1 complexes with difference cofactors. 32

CHAPTER I

INTRODUCTION

1.1 Background and rationale

Serine hydroxymethyltransferase (SHMT, EC 2.1.2.1), is an extensive enzyme that plays a role in the folate cycle of all prokaryotes and eukaryotes. The conversion of the reversible L-serine and tetrahydrofolate (THF) substrate by SHMT to glycine and 5,10-methylenetetrahydrofolate (MTHF) depends on a pyridoxal-5′-phosphate (PLP) cofactor which is covalently attached to the enzyme at the rest state [1, 2]. The MTHF product derived by SHMT serves a methyl group used for dUMP to dTMP in pyrimidine biosynthesis, and indirectly in purine biosynthesis via its conversion to 10-Formyl-THF (**Figure 1**) [2]. According to its important roles in nucleotide synthesis and its high expression level during cell proliferation of tumor and cancer cells [3], SHMT has been studied as a new attractive target for several diseases, such as cancers (i.e. breast, lung and colorectal cancer) [4-9] and malaria [4, 10-16]. In humans, there are two isoforms of SHMT including cytosolic SHMT (SHMT1) and mitochondrial SHMT (SHMT2), which share ~66% amino acid sequence identity [17]. Although some differences are observed, their similar structures exist as a homotetramer consisting of a single PLP cofactor in each monomer [2] (**Figure 2**). Moreover, the unique β-hairpin structure of human SHMT1 and SHMT2 is observed and known as a "flap motif" including 13 amino acids (^{273}VKSVDPKTGKEIL^{285}) [18]. This flap motif is reported to be the central role of SHMTs structural stabilization in tetramer as well as important for the binding affinity of THF and crucial for maintaining the dimer integrity for dimer– dimer assembly into tetramer [19]. SHMT1 increases essentially in rapid cell division such as cancer cells [20, 21], suggesting that this enzyme is more relevant to cancer drug target than SHMT2 [22, 23]. In addition, there are various crystal structures of SHMT2, while only one of the SHMT1 crystal structure is founded as depicted in **Figure 2** (PDB code 1BJ4) [2]. Therefore, the SHMT1 need to be studied. Each monomer comprises PLP covalently bound to Lys257 (PLP-Lys) in the SHMT1 binding pocket in the rest state [2, 24].

จุฬาลงกรณ์มหาวิทยาลัย
Chulalongkorn University

a

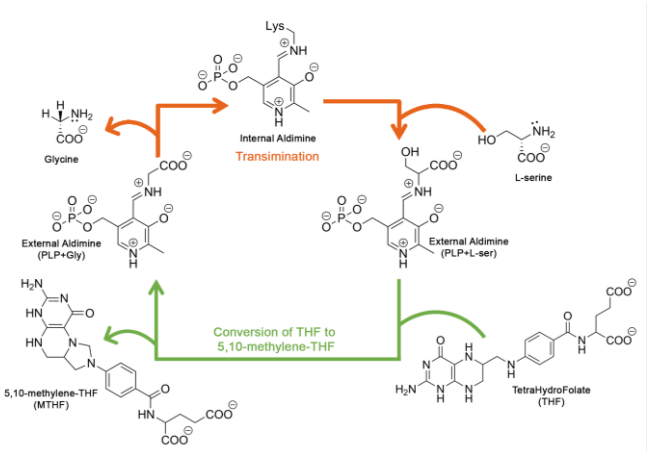

b

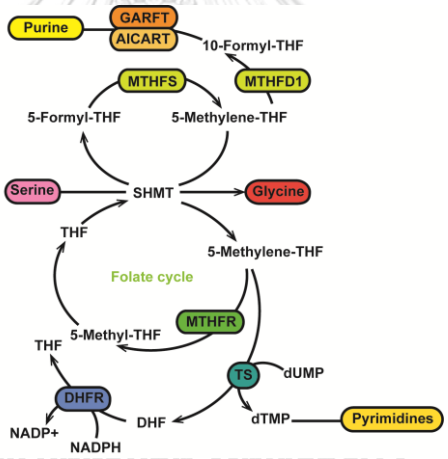

Figure 1 (a) The proposed schemes of serine hydroxymethyltransferase catalytic mechanism, which is the retro-aldol mechanism and **(b)** schematic overview of SHMT function, the cellular folate cycle involving SHMT, thymidylate synthase (TS), and dihydrofolate reductase (DHFR).

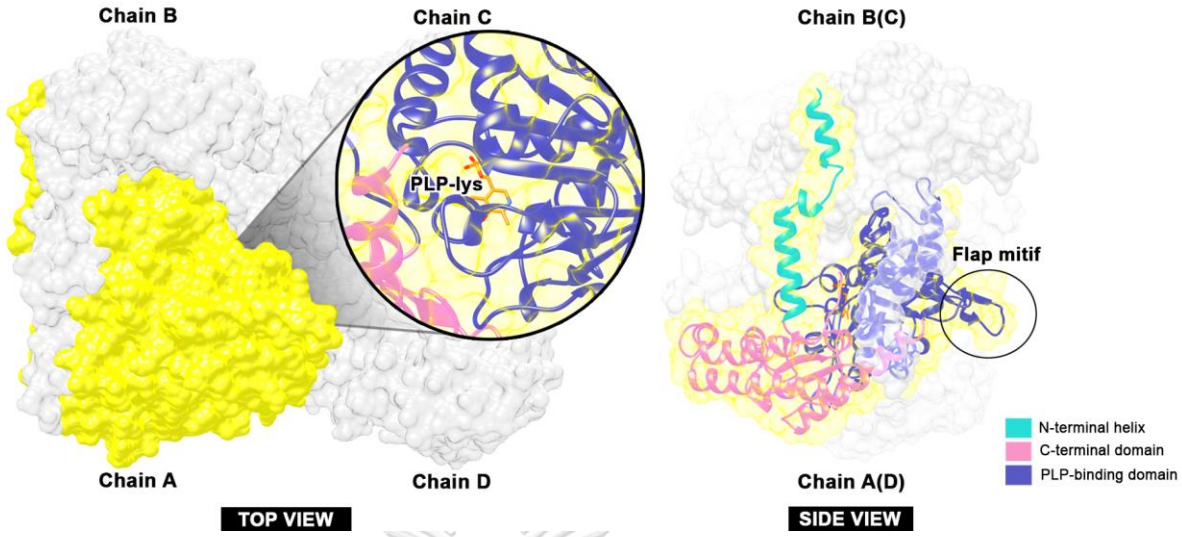

Figure 2 3D structure of tetrameric SHMT1 (PDB code 1BJ4) consist of a dimer (AB)–dimer (CD) association to form a native tetrameric quaternary structure [2]. The flap-connected region is located at the dimer interface (^{273}VKSVDPKTGKEIL^{285}).

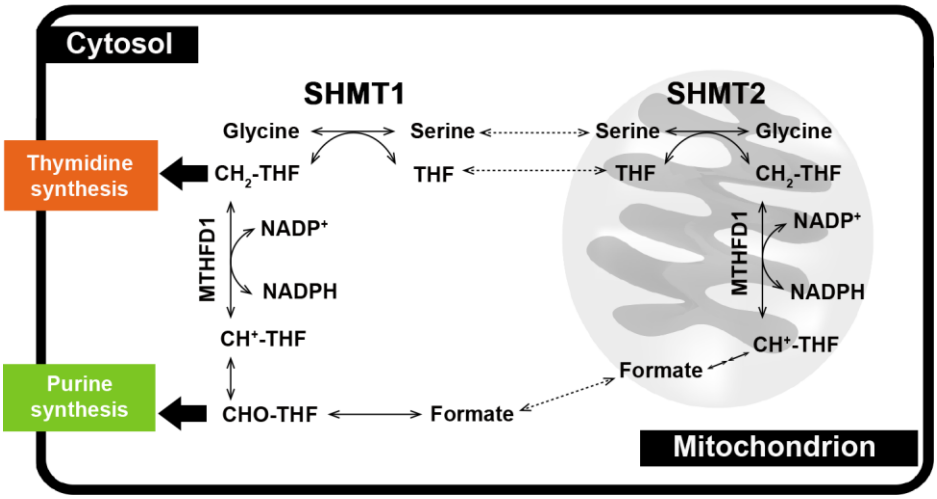

Figure 3 Compartmentalized One-Carbon Metabolism and Role of SHMT Cytosolic and Mitochondrial Isozymes

The scheme shows the reactions catalyzed by SHMT1 and SHMT1 in the context of the folate metabolism cycle taking place between the cytosol and mitochondria. The dead-end complexes responsible for the substrate inhibition

observed in this work and the structures of all substrates, products, and coenzymes are also shown.

SHMT2 is localized in mitochondria, where it plays a crucial role in the synthesis of glycine and formate; the latter is necessary for the biosynthesis of deoxythymidylate (dTMP) used in DNA replication [25, 26]. The other isoform, SHMT1, is mainly localized in the cytosol, although during the S phase of the cell cycle, it is imported together with SHMT2α in the nucleus, where it forms a complex with thymidylate synthase and dihydrofolate reductase (**Figure 3**). Given the distinct metabolic roles played by SHMT1 and SHMT2 in different cellular compartments, it is expected that the two isozymes might show different catalytic and regulation properties. However, very scarce information about SHMT2 is available[27, 28]. Most biochemical studies have been carried out on SHMT1.

1.2 Literature reviews

The SHMT1 activity has been reported by various experimental data without a clear understanding of the catalytic mechanism. A previous studied of the functional roles of the flap motif indicated that it is important for THF binding and controlling product release [19]. Meanwhile, optimum pH (6.5-8.5 pH) of various ligands, e.g., PLP-L-ser (PLS), PLP-Gly (PLG) and MTHF were used to perform the SHMT1 activity. There are two propose reaction mechanisms for the conversion of L-serine and THF to glycine and MTHF (**Figure 1a**) [29, 30]. The direct displacement mechanism is one of the possible reaction machanisms by which THF substrate can directly attack PLP-L-ser (PLS) without relevance of surrounding residues [31]. However, another scheme is suggested, the retro-aldo catalytic mechanism [30]. It is the most accepted scheme by the computational approach, quantum mechanics/molecular mechanics (QM/MM) method, rather than the direct displacement mechanism. Some amino acids (E57 of *Escherichia coli* [29] and H129 of *Plasmodium vivax* [30]) are two primary candidates for the role of the general base in the SHMT catalytic reaction [32-34] and water molecules in the binding pocket act as a general base and a general acid in the reaction with supporting of PLP cofactor [30]. Coot et al, [35] were investigated the

SHMT1 crystal structure that high binding efficiency of ligand was observed in the tetrameric form [19].

Table 1 Key amino acids in structural forming and function of SHMT which (') represent the residues from another chain.

Residues	Possible roles	References
Y'73	PLP binding	[32]
E'75	'open' to 'closed' form	[36]
Y'82	Inter subunit interaction	[36]
H148	Cofactor binding/stacking interaction	[37]
H151	Proton abstraction	[37]
D228	PLP interaction	[32]
H231	Enhance proton abstraction	[38]
K257	PLP binding/maintain oligomeric structure	[39]
R263	Distal interactions with PLP	[32]
R402	Substrate binding	[40]

จุฬาลงกรณ์มหาวิทยาลัย
CHULALONGKORN UNIVERSITY

Mutation of the residues that interact with PLP causes a range of disturbances in the oligomeric structure (mammalian SHMTs) and activity of SHMT. For example, K257 which involved in Schiff's base linkage with PLP as internal aldimine is crucial not only in catalysis but also in maintaining the tetrameric structure in sheep liver cytosolic recombinant SHMT (scSHMT) [39]. D228, which is H-bond to the pyridinium N is conserved not only in SHMT but in all fold type I PLP-dependent enzymes [32]. It is, therefore, not surprising that mutation of this residue (D227 in scSHMT) to N in scSHMT has serious consequences on the oligomeric structure of the tetrameric enzyme and catalytic activity [32]. The negative charge of D227 stabilizes the positive

charge of N1 of PLP and thereby enhances the function of PLP as an electron sink. This is a key feature in the function of all PLP-dependent enzymes irrespective of the reaction catalyzed. It is likely that D227 in scSHMT has a similar function. It could be postulated that the mutation of the corresponding residue in prokaryotic enzymes which would not result in loss of oligomeric structure would establish its role in catalysis. The histidine residues are conserved in prokaryotic and eukaryotic SHMTs [41] and were suggested to be essential for catalysis. Mutation of H148 affected cofactor binding/stacking interactions while H151 was indirectly involved in proton abstraction [37]. H231 is directly linked to O3 of PLP and facilitates the proton abstraction step [38]. Interestingly, a change in reaction specificity from a hydroxymethyl transfer to NADH oxidase reaction occurred when H231 was mutated to Y [42]. E'75 is essential for conversion of the enzyme from an 'open' to 'closed' form and is not involved in the proton abstraction step of catalysis. Y'82 stabilizes the quinonoid intermediate and R263 is probably essential for maintaining the geometry of the active site. The extensive mutational analysis and comparison of three-dimensional structures in this study has clarified the role of many amino acid residues present at the active site and the inter subunit contact regions of the enzyme. Structure determination of some of the mutant SHMT with substrates and characterization of the rate-limiting step in catalysis could further provide details in unraveling the reaction mechanism catalyzed by SHMT.

จุฬาลงกรณ์มหาวิทยาลัย
Chulalongkorn University

Crystal structure of human cytosolic SHMT was successfully solved at 2.65 Å (PDB code 1BJ4 [2]) and the structural comparison revealed that each subunit of the homotetrameric SHMT1 possesses a unique β-hairpin structure, or "flap motif" which contains 12 amino acids (^{274}KSVDPKTGKEIL^{285}) that are located on top of the tetrahydrofolate binding site. This flap motif is conserved only among the mammalian cytosolic SHMTs.

Figure 4 The crystal structure of human cytosolic serine hydroxymethyltransferase on the protein data bank (PDB code 1BJ4 [2])

The catalytic activity of this enzyme includes three stages. The first two stages are typical to all PLP-dependent enzymes and were already studied [6, 8]. The first stage involves the activation of the enzyme, in which the PLP cofactor becomes covalently bonded to an active site K257 residue, typically known as the internal aldimine (PLP-Lys). The second stage is triggered when the substrate is available, and it becomes covalently bonded to the PLP cofactor, forming the external aldimine (PLS or PLG). The third stage is what differentiates the PLP-dependent enzymes, and it is specific to each class of enzymes. In the case of SHMT, the enzyme catalyzes an α-elimination of L-ser that is subsequently inserted into the THF cofactor

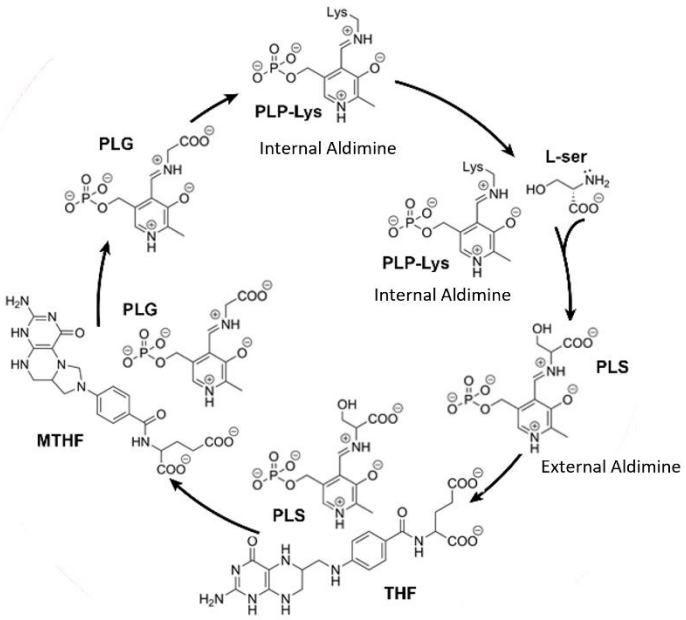

Figure 5 Representative scheme of the mechanism behind the internal and external aldimine formation of SHMT enzymes and the specific α-elimination reaction

The formaldehyde group is transferred from PLS to THF. One of the hypotheses suggests that the reaction occurs in one step, where nitrogen N1 of THF makes a nucleophilic attack on the Cβ of the L-Ser of PLS, promoting the α-elimination reaction. In the other hypothesis, the reaction requires two steps. The first step regulates the formation of a formaldehyde molecule (through the dissociation of the hydroxymethyl group from the external aldimine), which then undergoes a nucleophilic attack from nitrogen N1 of the THF cofactor [31]. These two hypotheses also diverge involves the protonation state of E75, which interacts very closely with the hydroxyl group of the external aldimine [31, 43, 44].

The experimental kinetic data is available for the human cytosolic SHMTs form of the role of the flap motif in controlling glycine release in THF-dependent catalysis by retaining THF binding. Therefore, the dissociation constant of THF was measured to validate the higher affinity of THF in the wild type SHMT1. THF can bind to both wild type SHMT1 and flap-deleted variant (SHMT1/Δflap) to form an Enzyme-THF binary complex with a maximum absorbance at 490 nm. The K_d values were calculated to be 108 ± 8 and 35 ± 8 μM for the SHMT1/Δflap and wild type SHMT1, respectively (**Figure 6**) [19].

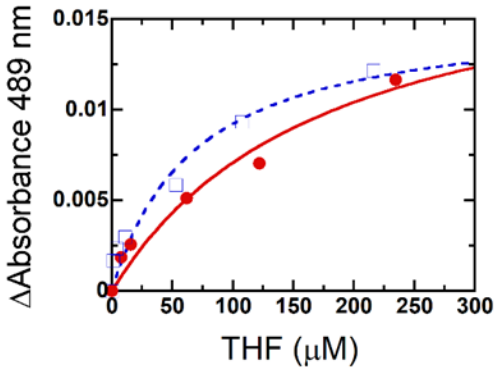

Figure 6 Comparison of THF binding to SHMT1/Δflap versus the wild-type enzyme.

The curve plot of absorbance change (ΔA) at 489 nm *versus* THF concentration for the binding reactions of SHMT1/Δflap (red solid line with filled circles) and wild-type (blue dashed line with empty squares) enzymes with various concentrations of THF (1-235 μM). The K_d values were determined accordingly as 180 ± 90 and 70 ± 30 μM, respectively [19].

1.3 Objective

The objective is to study the effect of wild-type SHMT1 with THF, MTHF, PLP-Lys, PLP-Ser and PLP-Gly bound in terms of structural stability and molecular dynamics behavior and binding affinities.

1.4 Scope of reserch

The structural stability, molecular dynamics behavior and binding affinities of wild type SHMT1 complexes will be investigated by means of MD simulation for 500 ns under NTP ensemble with a constant pressure of 1 atm at 298 K.

1.5 Research methodology

1. Literature review
   - Preparation of SHMT, THF, MTHF, PLP, PLS and PLG parameters by antechamber module
2. Build different models of SHMT complexes
   - Construct complexes structure of Tetrameric of SHMT1 including 6 systems for MD simulation
   - 6 systems including SHMT/PLP-Lys, SHMT/PLP-Lys/L-ser, SHMT/PLS, SHMT/PLS/THF, SHMT/PLG/MTHF and SHMT/PLG
3. Minimization: molecules were minimized with 3,000 steps of steepest descents (SD) and conjugated gradient (CG)
4. Heating: all systems were heated to temperature of 298K.
5. Simulate all systems with AMBER 16 at 298 K under NTP ensemble with a constant pressure of 1 atm for 500 ns
6. Analyze structural and dynamics properties

จุฬาลงกรณ์มหาวิทยาลัย
Chulalongkorn University

- Stability of all complexes by root mean square displacement (RMSD) calculation
- Stability of all complexes by B-factor calculation
- Binding free energy calculation for the focused systems

7. Summary, and thesis and publication preparations

1.6 Expected beneficial outcome(s)

The understanding of structural stability and binding free energy of SHMT/PLP-Lys, SHMT/PLP-Lys/L-ser, SHMT/PLS, SHMT/PLS/THF, SHMT/PLG/MTHF and SHMT/PLG complexes will be essential for future studies of mechanisms and the development of anticancer drugs.

จุฬาลงกรณ์มหาวิทยาลัย
CHULALONGKORN UNIVERSITY

CHAPTER II

THEORIES

2.1 Molecular dynamics (MD)

Molecular dynamics (MD) is another approach for the investigation of the atom location in space. In this approach, a single-point model is replaced by a dynamic model in which the nuclear system is forced into motion. The simulation of the motion is realized by the numerical solution of the classical Newtonian dynamic equations. The set of possible atom locations gives, for example, conformational ensemble profile for a given molecule. MD can also provide information on thermodynamic and dynamic properties of the molecules. The MD can be used for simulations of protein shapes and refinement of X-ray structures. MD simulations provide the ability to explain the dynamic aspects of a protein structure by tracking the time-dependent positions of all atoms in the system. The equations of motion follow Newton's second law [45]. Fundamentally, the acceleration of particles can be calculated by the first-order derivative of velocity (V_i) or second-order derivative of the atomic position (r_i) with respect to time t (eq.1).

$$F_i = m_i a_i = m\frac{dv_i}{dt^2} = m_i\frac{d^2 r_i}{dt^2} \quad (1)$$

จุฬาลงกรณ์มหาวิทยาลัย
CHULALONGKORN UNIVERSITY

Where F_i is the total force exerted on the particle i

m_i is mass of the particle i

a_i is acceleration of the particle i at

t is time

In addition, the external force acting on the particle i can be obtained from the negative gradient of potential energy (U) [45] as shown in eq. 2

$$F_i = -\frac{d}{d_{r_i}}U \quad (2)$$

The combination of mentioned equations leads us to (eq. 3)

$$F_i = -\frac{d}{d_{r_i}} U = m_i a_i = m\frac{dv_i}{dt^2} = m_i \frac{d^2 r_i}{dt^2} \quad (3)$$

In molecular system, the potential energy is the summation between the bonded and non-bonded interactions of particles. Bonded interactions compose of covalent bond-stretching, angle-bending, and dihedral angle potentials as described by harmonic oscillator function. Meanwhile, non-bonded interactions consist of electrostatic (ele) and van der Waals (vdW) interactions, which are described by coulomb potential and Lennard-Jones (L-J) potential, respectively. The sum of potential energy interaction can be expressed as follows:

$$U = E_{bonded} + E_{non-bonded} \quad (4)$$

$$U = (E_{bonds} + E_{angles} + E_{dihedrals})_{bonded} + (E_{ele} + E_{vdW})_{non-bonded} \quad (5)$$

$$U = \Sigma_{bonds}\frac{1}{2}k_b\left(r - r_{eq}\right)^2 + \Sigma_{angles}\frac{1}{2}k_\theta(\theta - \theta_{eq})^2 + \Sigma_{dihedrals}\frac{1}{2}V_n(1 + \cos(n\emptyset - \gamma)) + \Sigma_{i<j}^{atoms}\frac{q_i q_j}{Dr_{ij}}\left(\frac{A_{ij}}{r_{ij}^{12}} - \frac{B_{ij}}{r_{ij}^{6}}\right) \quad (6)$$

Where k_b is the force constants for bond-stretching

k_θ is the force constants for angle-bending

r_{eq} is the equilibrium bond length

θ_{eq} is bond angle

V_n is the height of rotational barrier

n is the periodicity of rotation

$\emptyset$ is the dihedral angle in the conformation of molecule in the phase shift angle, γ.

As previously mentioned, the non-bonded energy accounts for the electrostatic and van der Waals energies of the pair-wise sum of all possible interactions on atoms *i* and *j*. An electrostatic energy relies on the Coulomb's law which corresponds to the atomic charges, *qi* and *qj*, of atom *i* and *j*, respectively. Whereas *D* is the effective dielectric constant. The van der Waals interactions are

จุฬาลงกรณ์มหาวิทยาลัย
Chulalongkorn University

commonly used to describe steric interactions of molecule. Typically, the van der Waals energy is the sum of the attraction and repulsion between particles. The attractive interaction of van der Waals rapidly occurs in a short-range proportional to $1/r^6$ of the L-J potential. While the repulsion occurs with distance of interacting atoms become slightly less than the sum of their radius determined by the proportion of $1/r^{12}$. The A_{ij} and B_{ij} are constant factors which are dependent on the specific type of atom *i* and *j*. The position and velocity of atoms based on equation of motion can be calculated at time $t+\Delta t$.

In recent years it has seen significant developments in experimental techniques for studying the dynamic properties and MD modeling has been used regularly to provide atomic insights from these experiments. MD simulation plays an important role in increasing our understanding of the dynamics of protein structure [46].

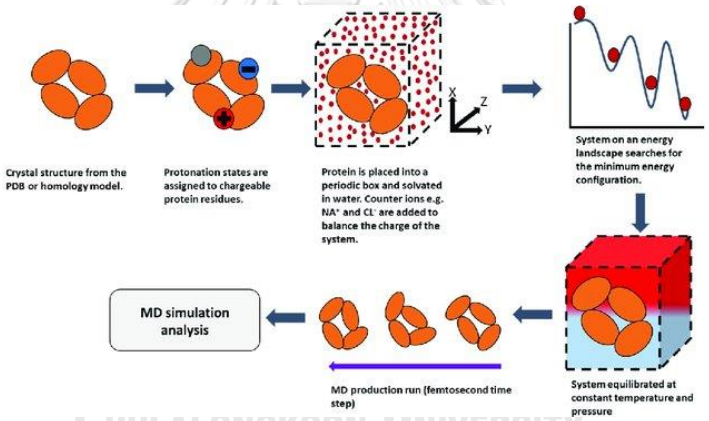

CHULALONGKORN UNIVERSITY

Figure 7 schematic of the molecular dynamics process [46].

The recent advancement in high-performance MD allows the creation of tens or hundreds of nanoseconds per day, allowing rapid rotation of medium-length MD simulations, including the production of a single long path. Therefore, these advances have new possibilities for using models to develop the atomic interpretation of experimental results and to create and test hypotheses for biomolecular functions [47]. Pharmacological targets such as protein kinases are interesting systems for such studies. Using long-time-scale MD simulation of the Abl

tyrosine kinase, Shan et al, 2009 performed the molecular details of a conformational change in the activation loop of the kinase [48, 49].

2.2 Basic Data Analysis

After a simulation has been completed, it needs to be analyzed to extract relevant information about the system of interest. This can be quite challenging and depends on the type of a simulated system. Here, a few common strategies for analyses will be outlined.

- Proteins

It is common to estimate the equilibrium of a protein simulation by computing the root mean squared deviation of the backbone atoms compared to the starting conformation,

$$RMSD = \sqrt{\frac{1}{N}\sum_{N}(r_i(t_0) - r_i(t))^2}$$

where N is the number of atoms, $r_i(t)$ the position of atom i, at time t. Prior to the analysis the protein needs to be fitted on to the starting structure to remove the overall translation and rotation. Although this is a straightforward analysis and gives an indication of local equilibrium, it is a far too simple method to assess the global convergence of the simulation. It is also possible to compute a pairwise RMSD between each snapshot in a simulation. This could for instance be used in order to evaluate how efficient the sampling has been, or if the simulation has become stuck in a local energy well. Whereas the RMSD provides an overall estimate for the entire protein and an approach to assess the degree of movement of individual residues is to compute the root mean squared fluctuation, which is simply the variance of the position of an atom:

$$RMSF = \frac{1}{T}\sum_{T}(r(t) - \bar{r})^2$$

where T is the total time of the simulation (or number of snapshots) and $\bar{r}$ is the average position. The RMSF can be related to the B-factor used in crystallography by multiplying by $8/3\pi$. The analysis can be done on a per residue-basis, where all the

จุฬาลงกรณ์มหาวิทยาลัย
Chulalongkorn University

atoms of a residue is included in the average and can for instance be used to assess the movement of sidechains. Alternatively, one can include only Ca atoms in the analysis to assess the backbone movement.

2.3 Binding free energy

- The Molecular Mechanics/Generalized Born Surface Area (MM/GBSA)

Methods that combine molecular mechanics energy and implicit solvation models, such as Molecular Mechanics/Generalized Born Surface Area (MM/GBSA), have been widely used in free energy calculations [50]. MM/GBSA calculation allows for free energy decomposition as well as energy contributions from different groups of atoms or types of interaction. For MM/GBSA, the binding free energy (ΔG_{bind}) between a ligand (L) and a receptor (R) to form a complex RL is calculated as following [51]:

$$\Delta G_{bind} = \Delta H - T\Delta S \approx \Delta E_{MM} + \Delta G_{sol} - T\Delta S \quad (1)$$

$$\Delta E_{MM} = \Delta E_{internal} + \Delta E_{electrostatic} + \Delta E_{vdW} \quad (2)$$

$$\Delta G_{sol} = \Delta G_{GB} + \Delta G_{SA} \quad (3)$$

Where ΔE_{MM}, ΔG_{sol}, and $-T\Delta S$ are the changes in the gas phase MM energy, the solvation free energy, and the conformational entropy, respectively. The ΔE_{MM} includes $\Delta E_{internal}$, which calculation from the bond, angle, and dihedral energies of the atom, $\Delta E_{electrostatic}$ and ΔE_{vdW} are electrostatic, and van der Waals energies. ΔG_{sol} is the sum of electrostatic solvation energy (polar contribution), ΔG_{GB}, and the nonelectrostatic solvation component (nonpolar contribution), ΔG_{SA} is the polar contribution is calculated using the PB model, whereas the nonpolar energy is estimated by solvent accessible surface area (SASA). The conformational entropy change $-T\Delta S$ is usually calculated by normal-mode analysis on a set of conformational snapshots taken from MD simulations [51]. Snapshots are taken from this single trajectory of MD. This simulation is used to calculate each free energy component in the above equations. The MM/PBSA have been effectively applied to a variety of protein-ligand [52] or protein-protein/peptide complexes [53], however, their performance is system dependent [54].

จุฬาลงกรณ์มหาวิทยาลัย
Chulalongkorn University

- Solvated interaction energy (SIE)

The solvated interaction energy (SIE) method belongs to the group of end-point force-field-based scoring functions that represent a reasonable compromise between time, computational resources, and accuracy. SIE approximates the protein–ligand binding free energy in aqueous solution (ΔG_{bind}) by an interaction energy contribution and a desolvation free energy contribution (ΔG_{dsolv}). Each of the interaction and desolvation contributions is further made up of an electrostatic component and a nonpolar component [55]:

$$\Delta G_{bind} \approx E_{inter} + \Delta G_{dsolv} = \left(E_{inter}^{Coul} + \Delta G_{dsolv}^{R}\right) + \left(E_{inter}^{vdW} + \Delta G_{dsolv}^{np}\right) \quad (5)$$

The specific functional form of the SIE function is given:

$$\Delta G_{bind} = \alpha \times [E_c(D_{in}) + \Delta G^R + E_{vdW} + \gamma \cdot \Delta MSA(\rho)] + C \quad (6)$$

Definitions of each term:

- E_c and E_{vdW} are the intermolecular Coulomb and van der Waals interaction energies in the bound state, separately.
- The term ΔG^R represents the change of the reaction energy induced by substrate bindings and was calculated by solving the Poisson equation with the boundary element method.
- The term $\gamma \cdot \Delta MSA$ represents the change of the molecular surface area upon bindings.
- The Amber van der Waals radii linear scaling coefficient(ρ), the solute interior dielectric constant (D_{in}), the molecular surface area coefficient (γ), the global proportionality coefficient related to the loss of conformational entropy upon binding (α) and a constant (C) are the parameters optimized by fitting to the absolute binding free energy for a set of 99 protein-ligand complex.

จุฬาลงกรณ์มหาวิทยาลัย
Chulalongkorn University

CHAPTER III
RESEARCH METHODOLOGY

3.1 Software

AMBER16, Discovery Studio 2019 Client, Chimera 1.14, GaussView 3.09, MobaXterm 9.4, VMD 1.9.2, OriginPro 8 and PDB2PQR 2.0.0 Server

3.2 Preparations of Ligands

- PLP covalent bond with K257 of SHMT1. The geometric optimization of PLP was performed at the HF/6-31(d) level of theory using Gaussian09 software [56-58]. The atomic charges of PLP were developed according to the standard procedure [59]. Additionally, the electrostatic potential (ESP) charges of each ligand were calculated with the same method. Subsequently, the restrained ESP (RESP) charges conversion was carried out from the ESP charges using the ANTECHAMBER module in the AMBER package. Afterwards the Prepgen program was used to link PLP cofactor with lysine257 of the SHMT1, generating a mainchain, which are characterized as having C_{α} of PLP to be connected to N of lysine257 residues. In the default setting, the program automatically generates the longest path as the mainchain.

- Preparations of L-ser, PLS, PLG, THF and MTHF. The geometric optimization of cofactors was performed at the HF/6- 31(d) level of theory using Gaussian09 program [56-58]. Therefore, the electrostatic potential (ESP) charges of each ligand were calculated at the same method. Subsequently, the restrained ESP (RESP) charges were carried out by converting from the ESP charges using the ANTECHAMBER module in AMBER package.

จุฬาลงกรณ์มหาวิทยาลัย
Chulalongkorn University

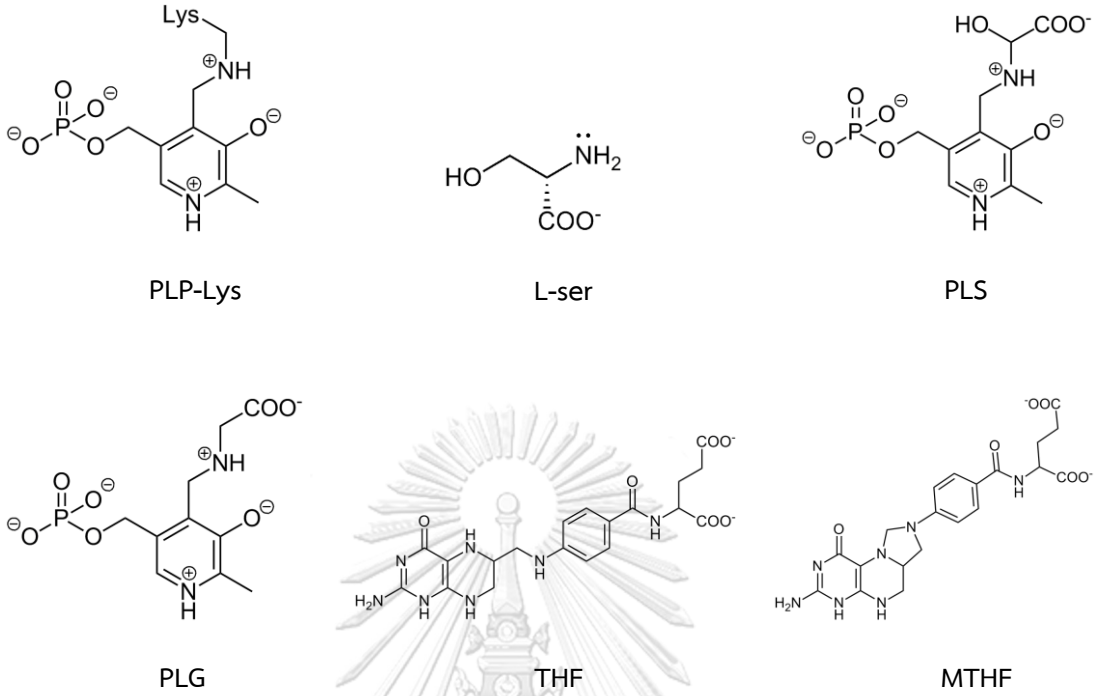

Figure 8 2D structure of the internal aldimine (PLP-Lys), L-serine (L-ser), pyridoxal-5'-Phosphate+L-ser (PLS), Pyridoxal-5'-Phosphate+glycine (PLG), tetrahydrofolate (THF) and 5,10- methylenetetrahydrofolate (MTHF)

3.3 Preparations of protein complexes

MD simulations of six model systems (**Figure 10**) were performed by using the AMBER 16 package program [57, 60, 61]. The starting configurations of SHMT with PLP covalently bound to K257 were taken from the Protein Data Bank (PDB code 1BJ4) in **Figure 9**. Noted that the model should be prepare for tetrameric models before MD simulation study. The protonation state at pH 7.0 of all ionizable residues was assigned by using PROPKA 3.1 program in PDB2PQR service Version 2.0.0 [62]. Then, all molecular dynamics simulations were carried out with the sander module in AMBER16. The ff14SB force field [63] was adopted for the protein and ligand (PLP-Lys, L-ser, PLS, PLG, THF and MTHF), while the atom types and the other molecular parameters of the ligands were assigned by generic AMBER force field version 2 (GAFF2) [64]. The missing hydrogen atoms were added using the Leap module in the

จุฬาลงกรณ์มหาวิทยาลัย
Chulalongkorn University

AMBER16 software [65]. Afterward, the hydrogen atoms of protein complexes were preliminarily minimized with 2500 steps of steepest descents (SD) method followed by 2500 steps of conjugated gradient (CG) method. Subsequently, the energy-minimized structures were solvated by ~23000 TIP3P water molecules in the truncated octahedral box with 10 Å cutoff and neutralized by the addition of Na+ ions. Noted that some crystallized water molecules were kept. After model solvation, the solvated models were minimized by the 2 steps described above under restraint on the protein atoms with the weight of 50.0 kcal/mol/Å^2, followed by the minimization on the whole system. The whole system was fully minimized using the mentioned minimization process. All covalent bonds involving hydrogen atoms were constrained using the SHAKE algorithm [66].

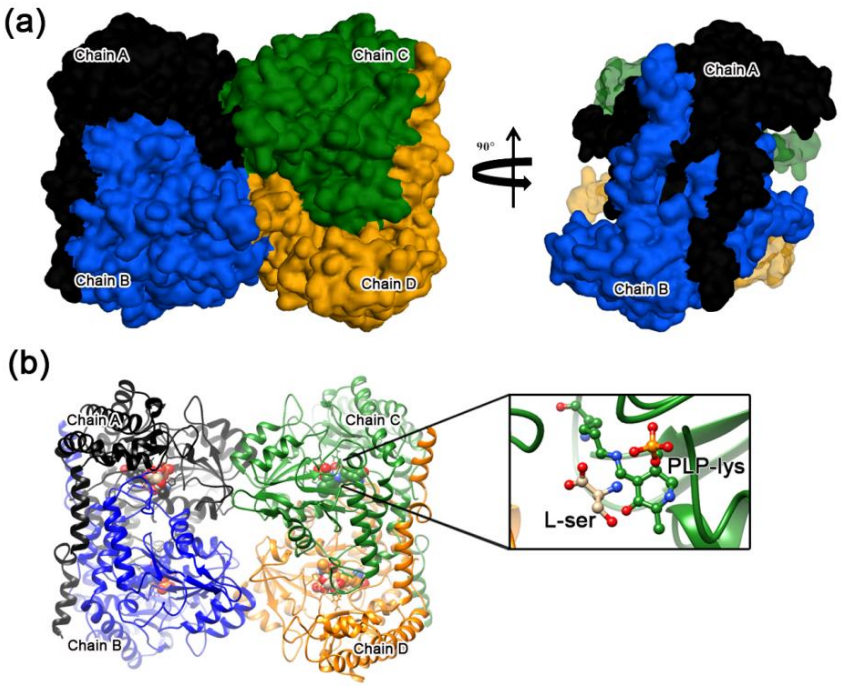

Figure 9 Structure of tetrameric SHMT1 **(a)** Surface representation showing vast inter-subunit interfaces within tight, vertically arranged dimers and contacts between the two dimers, where the secondary structure elements with the locations of PLP covalent bound with K257 (PLP-Lys) and L-ser are given in **(b)**.

- Systems

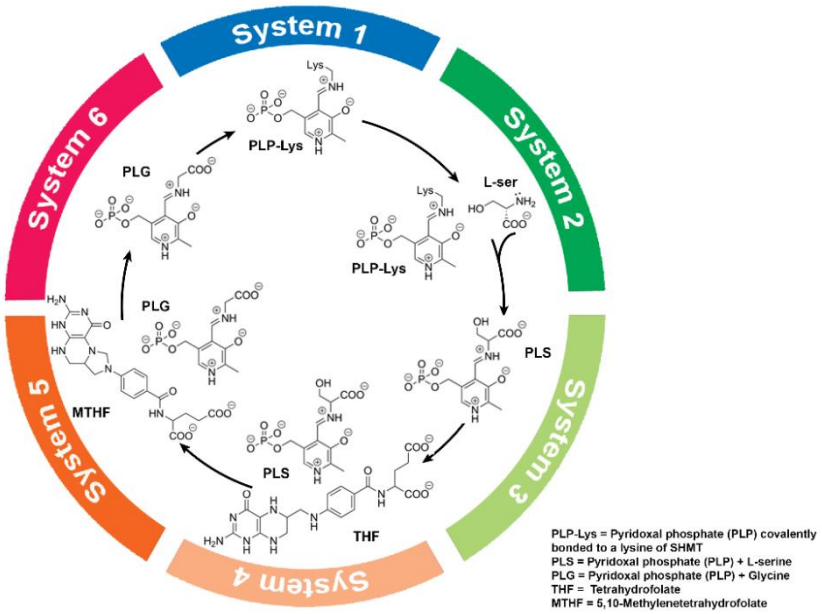

Figure 10 Six systems of SHMT1 from mechanism behind the internal and external aldimine formation for PLP-dependent enzymes and the specific α-elimination reaction [29].

3.4 Molecular dynamics (MD) simulations and analysis

All-atoms MD simulations of all six SHMT1 complexes were performed under periodic boundary condition using the pmemd CUDA in the AMBER16 [65] program packages for 500 ns. A cutoff of 12 Å was set for non-bonded interactions and the particle mesh Ewald (PME) method was employed for long-range electrostatic interactions. Temperature and pressure were controlled by the Berendsen algorithm [67]. The SHAKE algorithm was used to constrain all covalent bonds involving hydrogen atoms [66]. The simulated models were heated up from 10.0 K to 298.15 K with the relaxation time for 100 ps and were then equilibrated for another 100 ps. Subsequently, the simulations were carried out with NPT ensemble at 298.15 K and pressure of 1 atm for 500 ps. Afterward, the systems with full MD simulations were simulated for 500 ns, using 2 fs of integration time. A total of 50000 MD snapshots with equal time spacing over the course of the MD simulations were obtained.

The MD trajectories from the last 500 ns of the six independent simulations were extracted. By applying RMSD analysis the structural properties of each system were calculated using all atoms. The intermolecular H-Bond occupation, the number of contacts, and motion of protein were evaluated by the CPPTRAJ module [68]. Subsequently, the MD trajectories from the last 100 ns of the six independent simulations were extracted for ligand binding affinity and the per-residue decomposition free energy ($\Delta G_{bind}^{residue}$) calculation. Besides, the MD trajectories were recorded every 1000 steps. For the analysis within 10 Å of ligands, the MM-PBSA were calculated by MM/PBSA.py module [69]. The same sets of MD snapshots were used to predict the ΔG_{bind} based on the solvated interaction energy (SIE) method [70]. SIE is an end-point physics-based scoring function for predicting binding affinities in an aqueous solution, which is calculated by an interaction energy contribution, desolvation free energy contribution, electrostatic component and nonpolar component [70].

จุฬาลงกรณ์มหาวิทยาลัย
Chulalongkorn University

CHAPTER IV
RESULTS AND DISCUSSION

4.1 System stability of simulation models

- Root-mean square deviation (RMSD)

The binding behavior of six SHMT1 complexes were extensively studied by 500-ns MD simulations regarding the different cofactors, e.g., PLP-Lser, L-ser, PLS, PLG, THF and MTHF. In order to gain insight into the system stability of the complex, the root-mean square deviation (RMSD) for all-atom of SHMT1 and ligands were performed by comparing to those initial structures (**Figure 11**). All systems showed similar RMSD patterns at the first 50 ns. Subsequently, the RMSD values of complexes were continuously increased, and than maintained at a fluctuation of ~1.5-2.6 Å. However, the RMSD value of system 1 (SHMT1/PLP-Lys) was somewhat shaking at a fluctuation of ~1.8-2.9 Å. These results indicated that system 1 quite fluctuated along the 500-ns MD simulations compared to the another systems. This inactive form of PLP cofactor in system 1 might interfere the complex stability supporting by the experimental data [27].

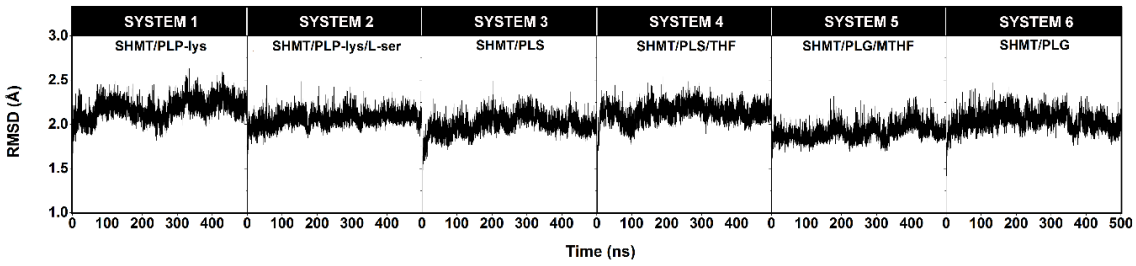

Figure 11 All-atom RMSDs of six SHMT1 complexes (black), including system1 (SHMT/PLP-Lys), system2 (SHMT/PLP-Lys/L-ser), system3 (SHMT/PLS), system4 (SHMT/PLS/THF), system5 (SHMT/PLG/MTHF) and system6 (SHMT/PLG).

- Number of hydrogen bond

Intermolecular hydrogen bond interaction is one of the essential interactions for stabilizing the ligand binding. In this research paper, the distance and angle of

hydrogen bond between donor and accepter atoms were used ≤ 3.5 Å and > 120 degree.

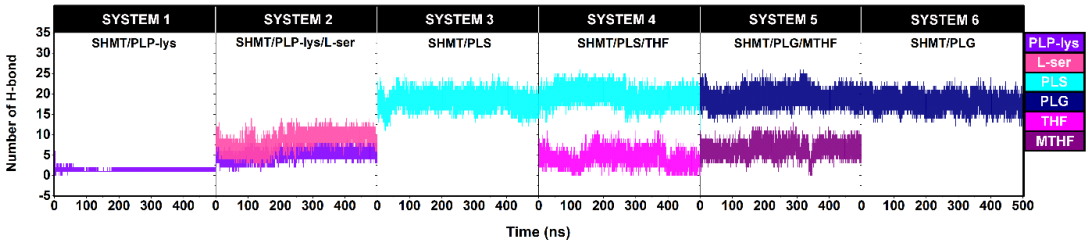

Figure 12 Number of hydrogen bond of SHMT1 performed in different cofactors, relative to their initial structures for the six studied systems: system1 (SHMT/PLP-Lys), system2 (SHMT/PLP-Lys/L-ser), system3 (SHMT/PLS), system4 (SHMT/PLS/THF), system5 (SHMT/PLG/MTHF), system6 (SHMT/PLG) within 3.5 Å cut-off distance of ligands cofactors along the simulations of 500 ns.

As a result, the number of hydrogen bonds interaction between system 1 and system 2, which PLP covalent bond with K257 of SHMT1 in the active site. The average number of H-bond of the PLP-Lys in system2 (~5 ± 1) was observed more than PLP-Lys of system1 (~1±1). Therefore, the L-ser could affect the binding ability of PLP-Lys in system 2. The phosphate group of PLP was proposed to interact with the substrate L-ser hydroxyl group and contributed to the critical intermediate formation and stereospecific orientation of formed quinonoid or carbanionic intermediates [71]. While the averages of the number of hydrogen bond interactions of PLS and PLG in each system are found similar levels as PLS in system3 (~18 ±2), PLS in system 4 (~18±5), PLG in system 5 (~19±1) and PLG in system 6 (~18 ±2). In addition, the number of H-bond interactions of THF in system 4 and MTHF in system 5 (~4± and ~6±1, respectively) were lower than the other four systems (systems 3-6 of PLS and PLG). Moreover, both PLS and PLG in each system are found average number H-bond interactions rather than THF and MTHF cofactors, which resulted from strong protein-ligand recognition within the cleft of the binding site. While THF and MTHF were less bound for hydrogen bond with SHMT1. This is because it binds to SHMT1 by a more non-covalent bond

จุฬาลงกรณ์มหาวิทยาลัย
Chulalongkorn University

- Number of contact atoms

define native contacts and a distance cutoff of 3.0 Å

to determine the mobility of the ligands (PLP-Lys, L-ser, PLS, PLG, THF and MTHF) in the SHMT1 pocket, the number of contact atoms was calculated by define native contacts and a distance cutoff of 3.0 Å. The PLS of system 4 gave higher average of contact atoms within SHMT1 (24 ± 4) than that PLS of system 3 (18. ± 5). Moreover, the average number of contacts atoms in system 5 (27± 5) was found higher than in system 6 (23 ± 4). Meanwhile, the average of contact atoms of THF in system 4A (13± 5) was found lower then the average of contact atoms of MTHF in system 5A (18± 5). Besides, the cofactors of THF and MTHF showed the average of the number of contact atoms lower than the other four systems (systems 3-6 of PLS and PLG). In addition, system 2 (SHMT/PLP-Lys/L-ser) showed the average number of contact atoms (24 ± 5) lower than system 1 (33± 3). Since some of the atoms in PLP-Lys could interact with L-ser. Thereby, the average of contact atoms of PLP-Lys in system 2 found lower number of contact atoms. Therefore, the system 5 showed highest of number of contact atoms while the system 2 showed lowest of number of contact atoms.

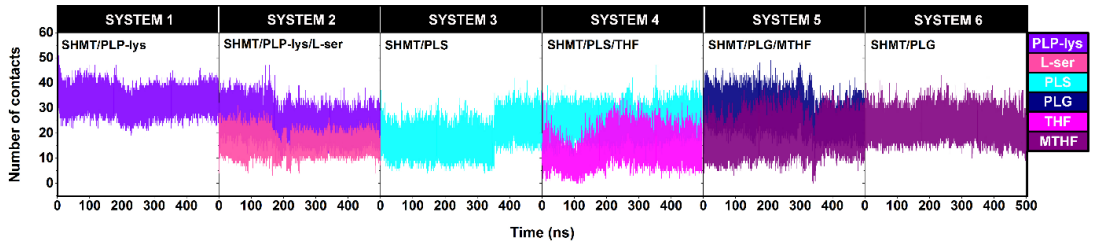

Figure 13 Number of contact atoms between SHMT1 with PLP-Lys, L-ser, PLS, PLG, THF and MTHF bound each system within 3.5 Å cut-off distance of ligands along the simulations of 500 ns

Altogether, the last 100 ns of each system reached an equilibrium state, which is supported by the RMSD, the number of hydrogen bonds and the number of contact atoms involved in ligands-protein interactions. Therefore, these MD

trajectories were selected for further analysis for the binding pattern at the molecular level.

- B-factor

To indicate protein flexibility and mobility, the B-factor was calculatedfor the backbone atoms of all minimized structures at the last 100-ns MD trajectories using the CPPTRAJ module and normalized in a relative scale. The results of the simulation showed the relationship between structural integrity and the B-factor, which indicates thermal motion of the molecules. The results demonstrate that the protein structure of the systems PLP covalent with K257 (system1 and 2) showed rigidity at the binding pocket and the whole structure was stable as shown in **Figure 14** Meanwhile, the system 3 (SHMT/PLS) and system4 (SHMT/PLS/THF) showed rigid movement at the binding site. Excerpt the C-terminal small domain of SHMT1 was the most flexible on system3 (without THF). Thus, THF cofactor may affect to stabilities of system. On the other hand, system 5 and system 6 (with and without MTHF cofactor respectively) showed stabilities within active site.

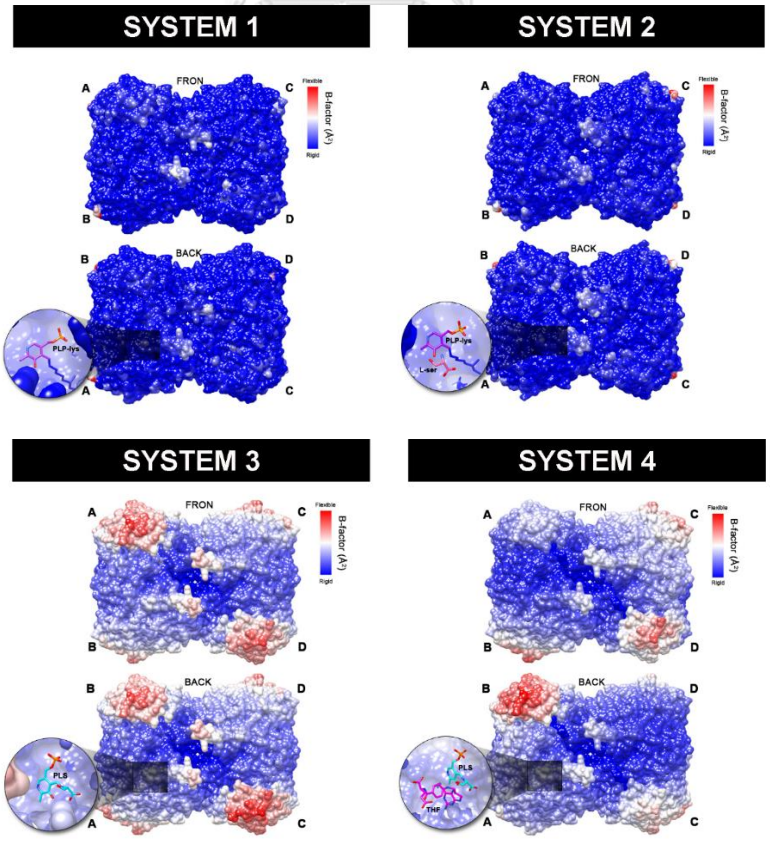

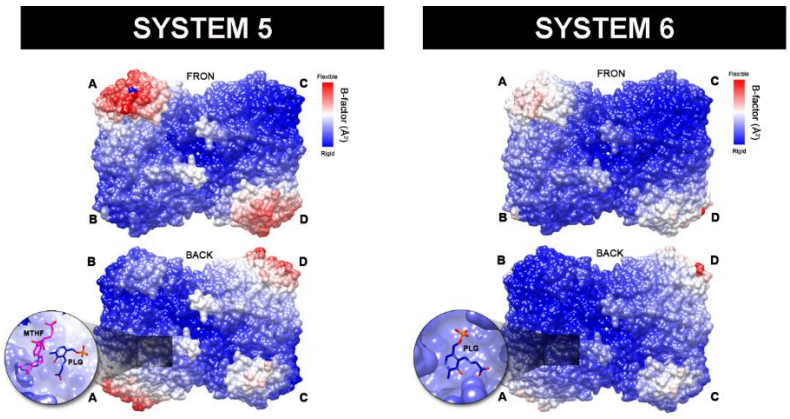

Figure 14 Normalized B-factor at last 100 ns MD simulation of SHMT1 complexes

- Distances between C7 atom of PLP-Lys and N atom of L-ser

To determine the occurrence of external aldimine (PLP bound with L-ser) the distance between C7 atom of PLP (covalently bound with K257) and N atom of L-ser along the simulation was investigated. The results showed that the distances between C7 atom in PLP-Lys and the N atom in L-ser was stable. Meanwhile, the distances between those atoms showed peaks around 2.8 to 5.5 Å along simulation of 500 ns and around 2.8-3.5 Å at last 100 ns **(Figure 15)**. This outcome suggesting that the distances between the C7 atom in PLP-Lys and the N atom in L-ser are in the position that might form the external aldimine

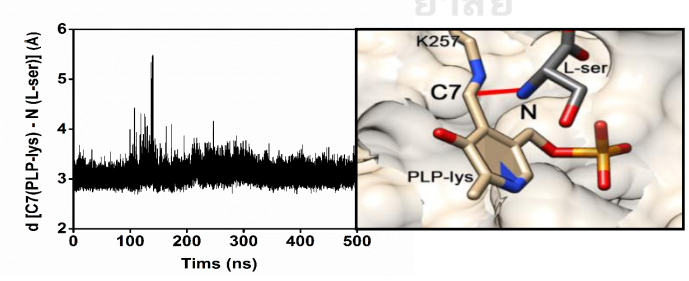

Figure 15 Distances between C7 atoms of PLP-Lys and N atom of L-ser along simulations

4.2 Intermolecular interactions of protein-ligand interface

The per-residue decomposition free energy ($\Delta G_{bind}^{residue}$) with 1000 snapshots based on MM/GBSA method and hydrogen bonding (H-bond) between protein and

ligands were analyzed for intermolecular interactions of protein-ligand interface. The residues which showed the energy contribution less than -1 kcal/mol and higher than 1 kcal/mol were considered and plotted in **Figure 16**. Using the sign (') presents residues of another chain.

In system 2, the L-ser was stabilized by the interaction of residues in the binding pocket, e.g., Y'73, S53, H148, H231, K257 and R402. In addition, the PLP (PLP-Lys) residues (-6.02 kcal/mol) was strongly stabilized with SHMT1/L-ser complex. The strong H-bond interaction of PLP was found in L-ser system 2. The 15 key residues, e.g., Y'73, Y'118, Q'301, S119, G120, S121, H148, T150, S203, D228, H231, H256, K257, R263 and R402 which interacted with PLS were found in system 3. Obviously, K257 showed the strongest binding affinity with PLS in system 3 (-16.92 kcal/mol). This is K257 residue are involved in Schiff's base linkage with PLP in an internal aldimine which acts as the nucleophile that forms the external aldimine product in this step in the SHMT1 [72, 73]. For systems 2 to 6, K257 was found in all five systems with lowest $\Delta G_{\text{bind}}^{\text{residue}}$ values (-2.05 kcal/mol for system 5, -2.32 kcal/mol for system 6 and -12.83 kcal/mol for system 4). Interestingly, PLS ligand of system 3 showed highly bind with K257. In systems 4, 5 and 6, the cofactors PLS and PLG were stabilized with the pocket site by interaction of Y'73, Q'301, G'302, Q'303, S53, S119, G120, S121, H148, T150, S203, D228, A230, H231, K257, R263 and R402. Interestingly, the PLS and PLG in each system ($\Delta G_{\text{bind}}^{\text{residue}}$ of -16.50, -20.51 and -21.18 kcal/mol for systems 4, 5 and 6, respectively) binds strongly to R263 residues. An examination of SHMT1 structure revealed that R263, a conserved residue in all SHMTs, could be involved in catalysis [2]. A position of R263 showed that the guanidino group of this residue strongly bond to PLS via the H-bond occupation ~70-100% with PLS and PLG in each system (percentage of H-bond of 99%, 84% and 98% for systems 4, 5 and 6, respectively). Therefore, this residue could be the key residue for PLS and PLG binding, which agree well in previously reported [26]. In addition, the major binding of these residues were electrostatic interactions (**Figure 17**). Furthermore, the system 5 (SHMT+MTHF/PLG) and system6 (SHMT/PLG) showed similar pattern of key residues interaction except the E'75 residue. E'75 was an early candidate for the general

จุฬาลงกรณ์มหาวิทยาลัย
Chulalongkorn University

base; however recent experimental data indicated that it is not involved in the proton abstraction [36, 43, 74]. Mutational analysis of E'75 in rabbit cytosolic serine hydroxymethyltransferase (rcSHMT) and E'74 (E'75 in SHMT1) in Sheep liver cytosolic SHMT (scSHMT) suggested that E'75 is involved in the condensation step instead of retro-aldol cleavage step [43]. In addition, structural studies suggested that E'75 could serve as the acid catalyst in the later steps but not for the retro-aldol mechanism [31], which is a critical residue in the binding of SHMT1 substrates. This residue can exist in both protonated [44, 75] and deprotonated forms [16]. In addition, the systems 4A (SHMT+PLS/THF) and 5A (SHMT+PLG/MTHF) have similarly low binding to SHMT1 (Y'82, L144, L149, F153, K157, K158, I160 and L396). The p-aminobenzoate ring of THF is stabilized the conserved **π-π** interaction of Y'82, the binding pocket from this part towards the l-glutamate group is distinguishable owing to the structural compactness of the SHMT homodimer and loop movement [18]. Interestingly, mutation of the corresponding residue Y82 to 'F' in scSHMT resulted in 95% loss in activity with cofactors did not yield the quinonoid intermediate [36]. These results suggest that Y'82 was involved in stabilizing the quinonoid intermediate [36]. Meanwhile, these ligands bind to SHMT1 by van der Waals interactions rather than electrostatic interactions (**Figure 17**).

The H-bond formation is one of the important factors that can determine the binding strength of ligand-protein interactions. The percentage of H-bond occupations at the last 100 ns of six systems were performed. The result showed the strong occupation of system 2 ranging from 71 to 100%, as illustrated in **Figure 16** with Y'73 (98%), S53 (99%), H148 (97%), H231 (92%), K257 (96%), R402 (87%) and PLP-Lys (99%) residues. PLS in system4 showed the H-bond stronger than PLS in system3. The strong H-bond bond of PLS with Y'73(100%), E'75(81%), G'303(94%), S53(98%), S119(99%), S121(99%), S203(78%), D228(83%), H231(99%), R263(99%), R402(99%) residues were obtained. While the H-bond bond of PLS in system3 was obtained as follows; S119(77%), S120(80%), H148(75%), D228(72%) and R402(75%). In addition, the interaction between THF and SHMT1 (system 4A) of each backbone atom showed a low value of H-bond occupation (10-32%). Meanwhile, the interaction between the MTHF cofactor and backbone of SHMT1 in system 5A

showed weak hydrogen bond occupation as well. The PLG of systems 5 and 6 showed a similar pattern of H-bond occupation indicated a strong H-bond consisting of Y'73, G'303, S119, G120, S121, D228, H231, R263 and R402. Noted that S53 in system6 showed the percentage of H-bond better than system 5, whereas T254 in system5 showed the H-bond interaction with the backbone of SHMT1 better than system 6. In contrast, the interaction of MTHF in the binding pocket showed weakly percentage of H-bond with SHMT1. Except for E'75 (84%) was bond tightly of hydrogen bond interaction with MTHF. Considering MTHF which is bound to the SHMT1/PLG complex, could be important for SHMT inhibitors [56]. Additionally, it has been proposed that THF substrate inhibition in SHMT1 may be linked to a particular flap motif made of residues 271–287 [4] because this is present in human SHMT1 but absent in *Plasmodium vivax* SHMT. However, this flap motif is also absent in *Escherichia coli* SHMT, which shows THF substrate inhibition [76].

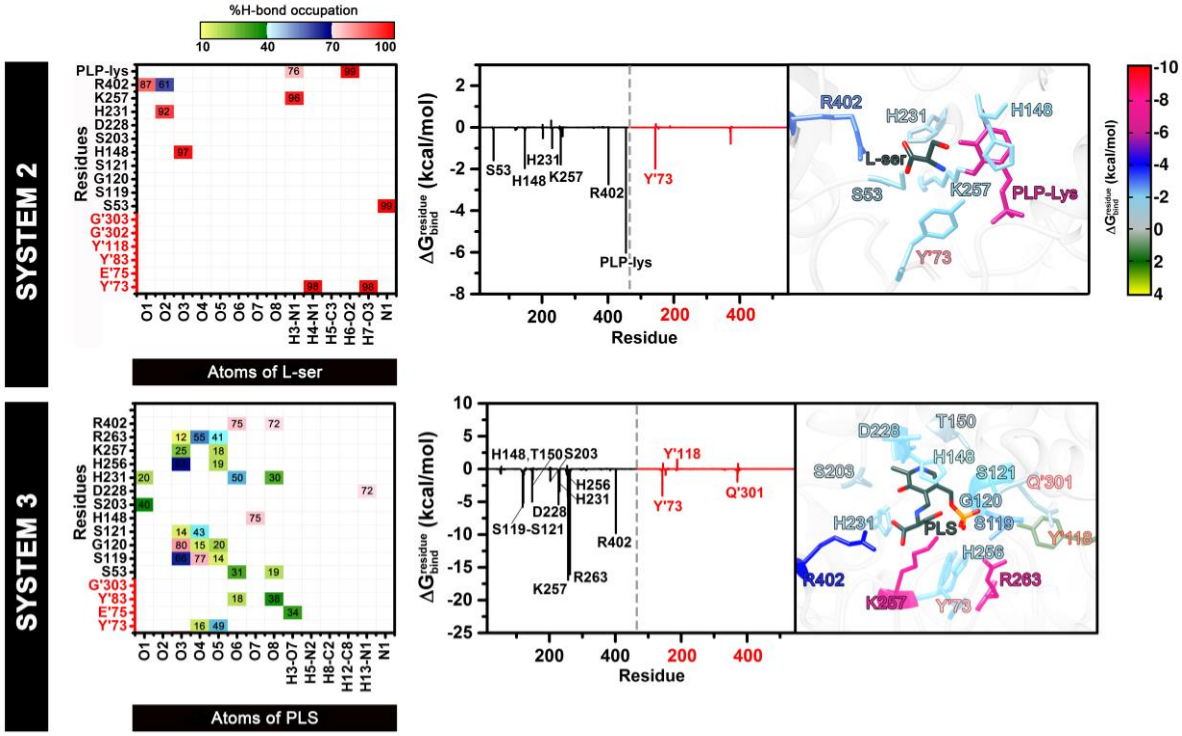

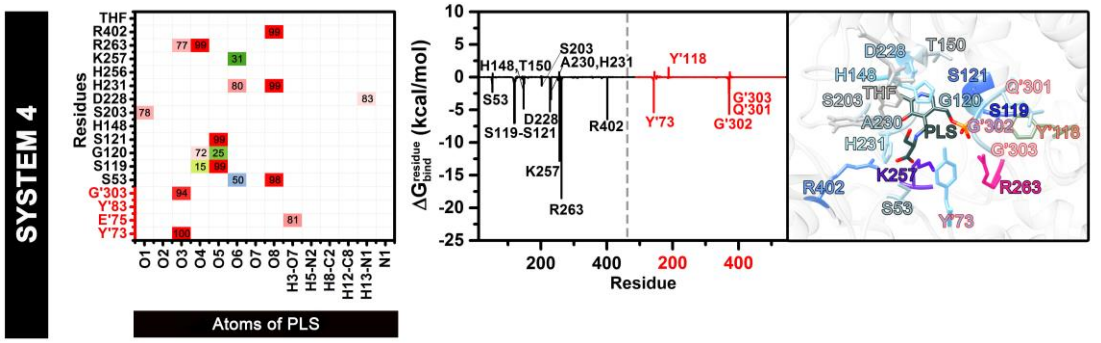

จุฬาลงกรณ์มหาวิทยาลัย
Chulalongkorn University

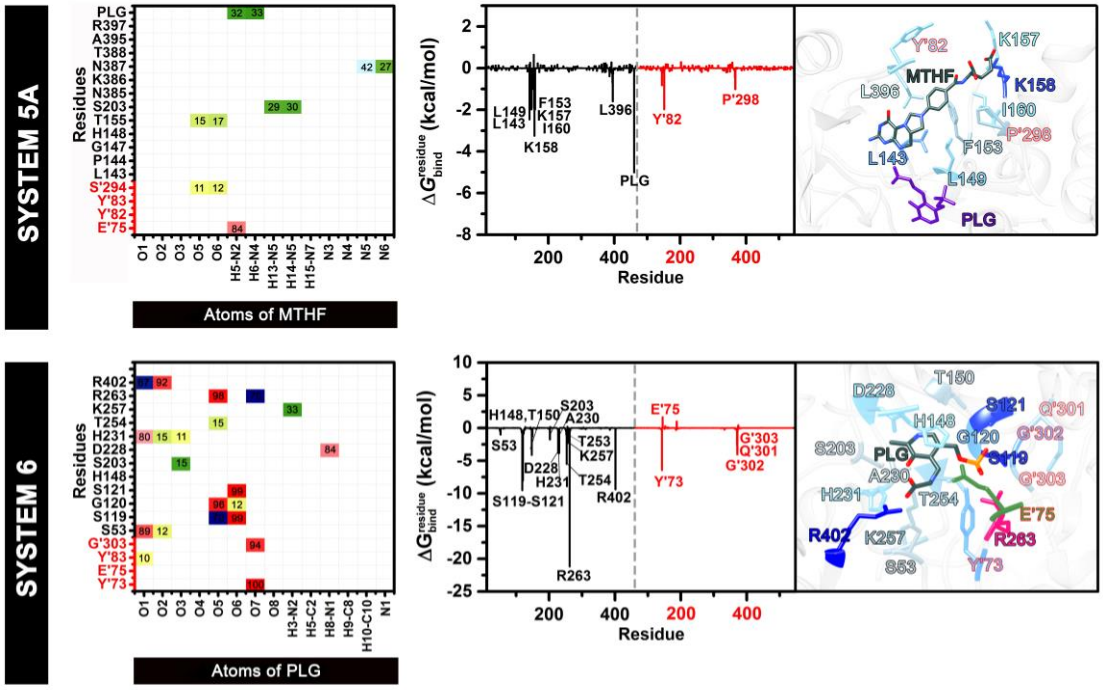

Figure 16 The percentage of H-bond occupation between ligand cofactors and SHMT1. The hydrogen bond strengths were divided into 3 levels including low (10-39%), moderate (40–69%), and strong (70–100%) interactions represented by the gradient of greenish, bluish and reddish grid cells, respectively (left). The per-residue energy (energy contribution cutoff ±1 kcal/mol) of SHMT1 complexes with difference cofactors. The important amino acids for ligand binding are shaded based on their decomposition energy, where the highest and lowest energies are ranging from green to red, respectively (right).

จุฬาลงกรณ์มหาวิทยาลัย
Chulalongkorn University

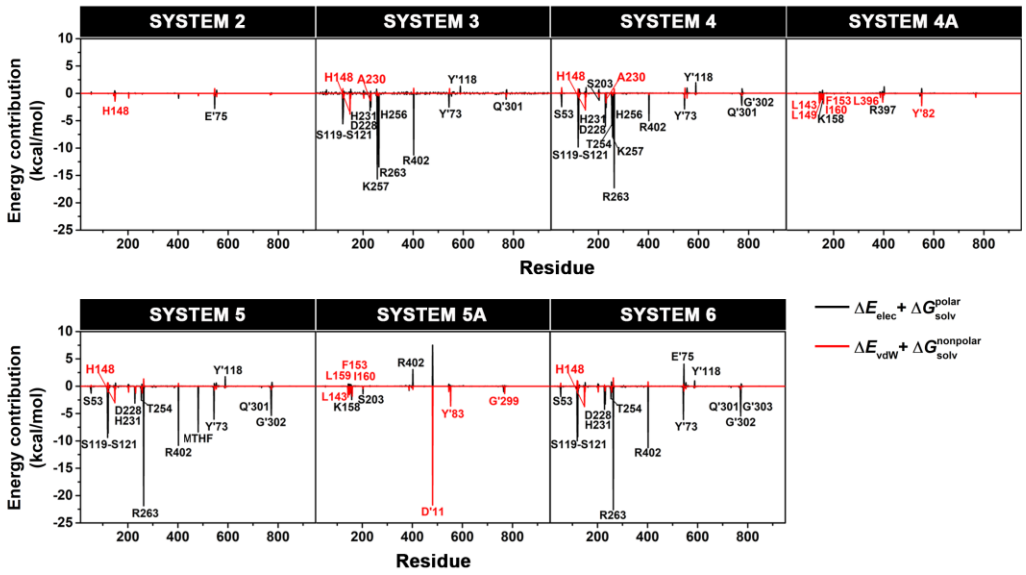

Figure 17 The electrostatic and van der Waals (vdW) energy contributions (energy contribution cutoff ±1 kcal/mol) of SHMT1 complexes with difference cofactors.

4.3 Ligand binding affinity

Based on solvated interaction energies (SIE) methods, an interaction energy contribution, desolvation free energy contribution, electrostatic component and nonpolar component of all six SHMT1s complexes were calculated and compared as showed in **Tables 2 and 3**. Among systems, the highest ΔG_{SIE} was observed in the SHMT+MTHF/PLG of system 5 (-15.01±0.06 kcal/mol). In addition, the THF (system 4A, -6.84±0.05 kcal/mol) showed low binding with SHMT1+PLS. Likewise, less binding of SHMT1+PLG with MTHF (system 5A, -7.96±0.05 kcal/mol) was obtained. Altogether, the interaction energy of each cofactor upon the mechanism against SHMT1 was ranged as follows; SHMT1+MTHF/PLG in system 5 (-15.01±0.06 kcal/mol) > SHMT1/PLS in system 3 (-14.88±0.02 kcal/mol) > SHMT1+THF/PLS in system 4 (-14.86±0.08 kcal/mol) > SHMT1/PLG in system 6 (-13.69±0.05 kcal/mol) > SHMT1+PLG/MTHF in system 5A (-7.96±0.05 kcal/mol) > SHMT1+PLS/THF in system 4A (-6.84±0.05 kcal/mol) > SHMT+PLP-Lys/L-ser in system 2 (-5.49±0.04 kcal/mol).

จุฬาลงกรณ์มหาวิทยาลัย
Chulalongkorn University

Table 2 Solvated interaction energy for L-ser, PLS and PLG complexes.

Energy component (kcal/mol)	System 2 SHMT1/PLP-Lys/L-ser	System 3 SHMT1/PLS	System 4 SHMT1+THF/PLS	System 5 SHMT1+MTHF/PLG	System 6 SHMT1/PLG
Inter vdW	-10.68±0.43	-25.66±0.16	-23.94±0.52	-23.22±0.49	-21.47±0.51
Inter Coulomb	-30.94±0.71	-231.31±0.23	-191.07±0.79	-219.39±0.54	-194.07±0.58
Reaction Field	19.65±0.34	149.64±0.14	108.42±0.39	134.08±0.33	119.19±0.34
Cavity	-2.87±0.01	-7.16±0.01	-7.66±0.02	-7.16±0.02	-6.78±0.02
Constant	-2.89				
α	0.10				
γ	0.01				
ΔG_{SIE}	-5.49±0.04	-14.88±0.02	-14.86±0.08	-15.01±0.06	-13.69±0.05
$\Delta G_{Exp.}$	-8.31 [78]	-7.93 [4]	-	-7.94 [79]	-7.48 [4]

Table 3 Solvated interaction energy for THF and MTHF complexes.

Energy component (kcal/mol)	System 4A SHMT+PLS/THF	System 5A SHMT+PLG/MTHF
Inter vdW	-37.37±0.31	-39.93±0.35
Inter Coulomb	-77.66±1.63	-112.02±1.36
Reaction Field	85.58±1.39	111.38±1.05
Cavity	-8.21±0.06	-7.82±0.07
Constant	-2.89	
α	0.10	
γ	0.01	
ΔG_{SIE}	-6.84±0.05	-7.96±0.05
$\Delta G_{Exp.}$	-	-9.77 [79]

จุฬาลงกรณ์มหาวิทยาลัย
Chulalongkorn University

CHAPTER V
CONCLUSIONS

This study focused on the reversible transfer mechanism of SHMT1 of one carbon atom from L-ser to tetrahydrofolate (THF), where the hydroxymethyl group is transferred from L-serine. The binding mechanism by classical molecular dynamics (MD) simulations and the binding free energy calculation of SHMT1-ligand complexes including PLP-Lys, PLS, PLG, THF and MTHF were elucidated and compared. According to the intermolecular interactions of cofactors of each system, the key residues, e.g., Y'73, S53, H231, K257, R263 and R402 were found generally in all systems. Moreover, PLS and PLG showed high binding affinity with R263 which involved in ligand stabilization. In addition, cofactors in each system showed a strong hydrogen bond with the S119 and G120 residues. The binding efficiency in term of SIE energy of all six SHMT1 complexes were estimated and compared. The results showed that the SIE value of SHMT+MTHF/PLG (system 5) > SHMT/PLS (system 3) > SHMT+THF/PLS (system 4) > SHMT/PLG (system 6) > SHMT+PLS/MTHF (system 5A) > SHMT+PLS/THF (system 4A) > SHMT/PLP-Lys/L-ser (system 2). Our results provided a better understanding of mechanisms of SHMT1 with various substrates. For example, it is possible that SHMT follows different mechanisms for catalysis depending on the substrate present. Therefore, understanding the chemistry of PLP-dependent reactions and the structure of specific SHMTs is necessary. The knowledge gained may lead to other applications of this enzyme such as stereospecific biocatalysis [80, 81]. These findings could be used as theoretical guidance for inhibitors developments towards SHMTs, which targeting anti-cancer inhibitors.

จุฬาลงกรณ์มหาวิทยาลัย
Chulalongkorn University

จุฬาลงกรณ์มหาวิทยาลัย
Chulalongkorn University

REFERENCES

1. Schirch, L., Serine hydroxymethyltransferase. Adv Enzymol Relat Areas Mol Biol, 1982. **53**: p. 83-112.
2. Renwick, S.B., K. Snell, and U. Baumann, The crystal structure of human cytosolic serine hydroxymethyltransferase: a target for cancer chemotherapy. Structure, 1998. **6**(9): p. 1105-16.
3. Locasale, J.W., Serine, glycine and one-carbon units: cancer metabolism in full circle. Nat Rev Cancer, 2013. **13**(8): p. 572-83.
4. Amornwatcharapong, W., et al., Human and Plasmodium serine hydroxymethyltransferases differ in rate-limiting steps and pH-dependent substrate inhibition behavior. Arch Biochem Biophys, 2017. **630**: p. 91-100.
5. Paiardini, A., et al., Screening and in vitro testing of antifolate inhibitors of human cytosolic serine hydroxymethyltransferase. ChemMedChem, 2015. **10**(3): p. 490-7.
6. Marani, M., et al., A pyrazolopyran derivative preferentially inhibits the activity of human cytosolic serine hydroxymethyltransferase and induces cell death in lung cancer cells. Oncotarget, 2016. **7**(4): p. 4570-83.
7. Paiardini, A., et al., Differential 3-bromopyruvate inhibition of cytosolic and mitochondrial human serine hydroxymethyltransferase isoforms, key enzymes in cancer metabolic reprogramming. Biochim Biophys Acta, 2016. **1864**(11): p. 1506-17.
8. Ducker, G.S., et al., Human SHMT inhibitors reveal defective glycine import as a targetable metabolic vulnerability of diffuse large B-cell lymphoma. Proc Natl Acad Sci U S A, 2017. **114**(43): p. 11404-11409.
9. Chen, J., et al., The loss of SHMT2 mediates 5-fluorouracil chemoresistance in colorectal cancer by upregulating autophagy. Oncogene, 2021. **40**(23): p. 3974-3988.
10. Nirmalan, N., et al., Transcriptional analysis of genes encoding enzymes of the folate pathway in the human malaria parasite Plasmodium falciparum. Mol

จุฬาลงกรณ์มหาวิทยาลัย
Chulalongkorn University

Microbiol, 2002. **46**(1): p. 179-90.

11. Leartsakulpanich, U., et al., Cloning and characterization of Plasmodium vivax serine hydroxymethyltransferase. Parasitol Int, 2008. **57**(2): p. 223-8.
12. Maenpuen, S., et al., Characterization of Plasmodium falciparum serine hydroxymethyltransferase—A potential antimalarial target. Molecular and Biochemical Parasitology, 2009. **168**(1): p. 63-73.
13. Pornthanakasem, W., et al., Plasmodium serine hydroxymethyltransferase: indispensability and display of distinct localization. Malar J, 2012. **11**: p. 387.
14. Witschel, M.C., et al., Inhibitors of plasmodial serine hydroxymethyltransferase (SHMT): cocrystal structures of pyrazolopyrans with potent blood- and liver-stage activities. J Med Chem, 2015. **58**(7): p. 3117-30.
15. Schwertz, G., et al., Antimalarial Inhibitors Targeting Serine Hydroxymethyltransferase (SHMT) with in Vivo Efficacy and Analysis of their Binding Mode Based on X-ray Cocrystal Structures. Journal of Medicinal Chemistry, 2017. **60**(12): p. 4840-4860.
16. Schwertz, G., et al., Conformational Aspects in the Design of Inhibitors for Serine Hydroxymethyltransferase (SHMT): Biphenyl, Aryl Sulfonamide, and Aryl Sulfone Motifs. Chemistry, 2017. **23**(57): p. 14345-14357.
17. Garrow, T.A., et al., Cloning of human cDNAs encoding mitochondrial and cytosolic serine hydroxymethyltransferases and chromosomal localization. J Biol Chem, 1993. **268**(16): p. 11910-6.
18. Chitnumsub, P., et al., The structure of Plasmodium falciparum serine hydroxymethyltransferase reveals a novel redox switch that regulates its activities. Acta Crystallographica Section D, 2014. **70**(6): p. 1517-1527.
19. Ubonprasert, S., et al., A flap motif in human serine hydroxymethyltransferase is important for structural stabilization, ligand binding, and control of product release. The Journal of biological chemistry, 2019. **294**(27): p. 10490-10502.
20. Eichler, H.G., R. Hubbard, and K. Snell, The role of serine hydroxymethyltransferase in cell proliferation: DNA synthesis from serine following mitogenic stimulation of lymphocytes. Biosci Rep, 1981. **1**(2): p. 101-6.
21. Thorndike, J., T.T. Pelliniemi, and W.S. Beck, Serine hydroxymethyltransferase

จุฬาลงกรณ์มหาวิทยาลัย
Chulalongkorn University

activity and serine incorporation in leukocytes. Cancer Res, 1979. **39**(9): p. 3435-40.

22. Rao, N.A., R. Talwar, and H.S. Savithri, Molecular organization, catalytic mechanism and function of serine hydroxymethyltransferase--a potential target for cancer chemotherapy. Int J Biochem Cell Biol, 2000. **32**(4): p. 405-16.
23. Agrawal, S., et al., Cloning, expression, activity and folding studies of serine hydroxymethyltransferase: a target enzyme for cancer chemotherapy. J Mol Microbiol Biotechnol, 2003. **6**(2): p. 67-75.
24. Cerqueira, N.M.F.S.A., P.A. Fernandes, and M.J. Ramos, Computational Mechanistic Studies Addressed to the Transimination Reaction Present in All Pyridoxal 5′-Phosphate-Requiring Enzymes. Journal of Chemical Theory and Computation, 2011. **7**(5): p. 1356-1368.
25. Pfendner, W. and L.I. Pizer, The metabolism of serine and glycine in mutant lines of Chinese hamster ovary cells. Arch Biochem Biophys, 1980. **200**(2): p. 503-12.
26. Anderson, D.D., C.M. Quintero, and P.J. Stover, Identification of a de novo thymidylate biosynthesis pathway in mammalian mitochondria. Proceedings of the National Academy of Sciences, 2011. **108**(37): p. 15163.
27. Giardina, G., et al., How pyridoxal 5'-phosphate differentially regulates human cytosolic and mitochondrial serine hydroxymethyltransferase oligomeric state. Febs j, 2015. **282**(7): p. 1225-41.
28. Schirch, L. and D. Peterson, Purification and properties of mitochondrial serine hydroxymethyltransferase. J Biol Chem, 1980. **255**(16): p. 7801-6.
29. Fernandes, H.S., M.J. Ramos, and N.M.F.S.A. Cerqueira, Catalytic Mechanism of the Serine Hydroxymethyltransferase: A Computational ONIOM QM/MM Study. ACS Catalysis, 2018. **8**(11): p. 10096-10110.
30. Santatiwongchai, J., D. Gleeson, and M.P. Gleeson, Theoretical Evaluation of the Reaction Mechanism of Serine Hydroxymethyltransferase. The Journal of Physical Chemistry B, 2019. **123**(2): p. 407-418.
31. Schirch, V. and D.M. Szebenyi, Serine hydroxymethyltransferase revisited. Curr Opin Chem Biol, 2005. **9**(5): p. 482-7.

จุฬาลงกรณ์มหาวิทยาลัย
Chulalongkorn University

32. Trivedi, V., et al., Crystal Structure of Binary and Ternary Complexes of Serine Hydroxymethyltransferase from Bacillus stearothermophilus: INSIGHTS INTO THE CATALYTIC MECHANISM *. Journal of Biological Chemistry, 2002. **277**(19): p. 17161-17169.

33. Chiba, Y., et al., Mechanism for folate-independent aldolase reaction catalyzed by serine hydroxymethyltransferase. Febs j, 2012. **279**(3): p. 504-14.

34. Appaji Rao, N., et al., Structure-function relationship in serine hydroxymethyltransferase. Biochim Biophys Acta, 2003. **1647**(1-2): p. 24-9.

35. Emsley, P. and K. Cowtan, Coot: model-building tools for molecular graphics. Acta Crystallogr D Biol Crystallogr, 2004. **60**(Pt 12 Pt 1): p. 2126-32.

36. Rao, J.V., et al., The role of Glu74 and Tyr82 in the reaction catalyzed by sheep liver cytosolic serine hydroxymethyltransferase. Eur J Biochem, 2000. **267**(19): p. 5967-76.

37. Jagath, J.R., et al., The Role of His-134, -147, and -150 Residues in Subunit Assembly, Cofactor Binding, and Catalysis of Sheep Liver Cytosolic Serine Hydroxymethyltransferase *. Journal of Biological Chemistry, 1997. **272**(39): p. 24355-24362.

38. Talwar, R., et al., His230 of serine hydroxymethyltransferase facilitates the proton abstraction step in catalysis. European journal of biochemistry, 2000. **267**(5): p. 1441-1446.

39. Talwar, R., et al., The role of lysine-256 in the structure and function of sheep liver recombinant serine hydroxymethyltransferase. Acta Biochim Pol, 1997. **44**(4): p. 679-88.

40. Jagath, J.R., N.A. Rao, and H.S. Savithri, Role of Arg-401 of cytosolic serine hydroxymethyltransferase in subunit assembly and interaction with the substrate carboxy group. The Biochemical journal, 1997. **327 (Pt 3)**(Pt 3): p. 877-882.

41. Usha, R., H.S. Savithri, and N. Appaji Rao, The primary structure of sheep liver cytosolic serine hydroxymethyltransferase and an analysis of the evolutionary relationships among serine hydroxymethyltransferases. Biochimica et Biophysica Acta (BBA) - Protein Structure and Molecular Enzymology, 1994. **1204**(1): p. 75-

จุฬาลงกรณ์มหาวิทยาลัย
Chulalongkorn University

83.

42. Talwar, R., N.A. Rao, and H.S. Savithri, A change in reaction specificity of sheep liver serine hydroxymethyltransferase. Induction of NADH oxidation upon mutation of His230 to Tyr. Eur J Biochem, 2000. **267**(4): p. 929-34.

43. Szebenyi, D.M.E., et al., Serine Hydroxymethyltransferase: Role of Glu75 and Evidence that Serine Is Cleaved by a Retroaldol Mechanism. Biochemistry, 2004. **43**(22): p. 6865-6876.

44. Scarsdale, J.N., et al., Crystal structure at 2.4 A resolution of E. coli serine hydroxymethyltransferase in complex with glycine substrate and 5-formyl tetrahydrofolate. J Mol Biol, 2000. **296**(1): p. 155-68.

45. van Gunsteren, W.F. and H.J.C. Berendsen, Computer Simulation of Molecular Dynamics: Methodology, Applications, and Perspectives in Chemistry. Angewandte Chemie International Edition in English, 1990. **29**(9): p. 992-1023.

46. Hollingsworth, S.A. and R.O. Dror, Molecular Dynamics Simulation for All. Neuron, 2018. **99**(6): p. 1129-1143.

47. Hata, H., M. Nishiyama, and A. Kitao, Molecular dynamics simulation of proteins under high pressure: Structure, function and thermodynamics. Biochim Biophys Acta Gen Subj, 2020. **1864**(2): p. 129395.

48. Klepeis, J.L., et al., Long-timescale molecular dynamics simulations of protein structure and function. Curr Opin Struct Biol, 2009. **19**(2): p. 120-7.

49. Shan, Y., et al., A conserved protonation-dependent switch controls drug binding in the Abl kinase. Proc Natl Acad Sci U S A, 2009. **106**(1): p. 139-44.

50. Wang, J.M., T. Hou, and X. Xu, Recent advances in free energy calculations with a combination of molecular mechanics and continuum models. Current Computer-Aided Drug Design, 2006. **2**(3): p. 287-306.

51. Hou, T., et al., Assessing the performance of the MM/PBSA and MM/GBSA methods. 1. The accuracy of binding free energy calculations based on molecular dynamics simulations. J Chem Inf Model, 2011. **51**(1): p. 69-82.

52. Hou, T., S. Guo, and X. Xu, Predictions of Binding of a Diverse Set of Ligands to Gelatinase-A by a Combination of Molecular Dynamics and Continuum Solvent

จุฬาลงกรณ์มหาวิทยาลัย
Chulalongkorn University

Models. The Journal of Physical Chemistry B, 2002. **106**(21): p. 5527-5535.

53. Wang, W. and P.A. Kollman, Free energy calculations on dimer stability of the HIV protease using molecular dynamics and a continuum solvent model. J Mol Biol, 2000. **303**(4): p. 567-82.

54. Pearlman, D.A., Evaluating the molecular mechanics poisson-boltzmann surface area free energy method using a congeneric series of ligands to p38 MAP kinase. J Med Chem, 2005. **48**(24): p. 7796-807.

55. Sulea, T., Q. Cui, and E.O. Purisima, Solvated Interaction Energy (SIE) for Scoring Protein–Ligand Binding Affinities. 2. Benchmark in the CSAR-2010 Scoring Exercise. Journal of Chemical Information and Modeling, 2011. **51**(9): p. 2066-2081.

56. Mahalapbutr, P., et al., A theoretical study on the molecular encapsulation of luteolin and pinocembrin with various derivatized beta-cyclodextrins. Journal of Molecular Structure, 2019. **1180**: p. 480-490.

57. Sanachai, K., et al., Insights into the Binding Recognition and Susceptibility of Tofacitinib toward Janus Kinases. ACS Omega, 2020. **5**(1): p. 369-377.

58. Kammarabutr, J., et al., Low susceptibility of asunaprevir towards R155K and D168A point mutations in HCV NS3/4A protease: A molecular dynamics simulation. J Mol Graph Model, 2019. **89**: p. 122-130.

59. Jala, V.R., et al., Overexpression and characterization of dimeric and tetrameric forms of recombinant serine hydroxymethyltransferase fromBacillus stearothermophilus. Journal of Biosciences, 2002. **27**(3): p. 233-242.

60. Mahalapbutr, P., et al., Molecular insights into inclusion complexes of mansonone E and H enantiomers with various beta-cyclodextrins. J Mol Graph Model, 2018. **79**: p. 72-80.

61. Phanich, J., et al., Role of R292K mutation in influenza H7N9 neuraminidase toward oseltamivir susceptibility: MD and MM/PB(GB)SA study. J Comput Aided Mol Des, 2016. **30**(10): p. 917-926.

62. Dolinsky, T.J., et al., PDB2PQR: an automated pipeline for the setup of Poisson–Boltzmann electrostatics calculations. Nucleic Acids Research, 2004. **32**(suppl_2): p. W665-W667.

จุฬาลงกรณ์มหาวิทยาลัย
Chulalongkorn University

63. Maier, J.A., et al., ff14SB: Improving the Accuracy of Protein Side Chain and Backbone Parameters from ff99SB. Journal of Chemical Theory and Computation, 2015. **11**(8): p. 3696-3713.

64. Wang, J., et al., Development and testing of a general amber force field. J Comput Chem, 2004. **25**(9): p. 1157-74.

65. Gotz, A.W., et al., Routine Microsecond Molecular Dynamics Simulations with AMBER on GPUs. 1. Generalized Born. J Chem Theory Comput, 2012. **8**(5): p. 1542-1555.

66. Hess, B., et al., LINCS: A Linear Constraint Solver for molecular simulations. Journal of Computational Chemistry, 1998. **18**.

67. Hünenberger, P.H., Thermostat Algorithms for Molecular Dynamics Simulations, in Advanced Computer Simulation. 2005. p. 105-149.

68. Roe, D.R. and T.E. Cheatham, PTRAJ and CPPTRAJ: Software for Processing and Analysis of Molecular Dynamics Trajectory Data. Journal of Chemical Theory and Computation, 2013. **9**(7): p. 3084-3095.

69. Genheden, S. and U. Ryde, The MM/PBSA and MM/GBSA methods to estimate ligand-binding affinities. Expert opinion on drug discovery, 2015. **10**(5): p. 449-461.

70. Naïm, M., et al., Solvated Interaction Energy (SIE) for Scoring Protein–Ligand Binding Affinities. 1. Exploring the Parameter Space. Journal of Chemical Information and Modeling, 2007. **47**(1): p. 122-133.

71. Beattie, A.E., et al., Reconstitution of the pyridoxal 5′-phosphate (PLP) dependent enzyme serine palmitoyltransferase (SPT) with pyridoxal reveals a crucial role for the phosphate during catalysis. Chemical Communications, 2013. **49**(63): p. 7058-7060.

72. Scarsdale, J.N., et al., Crystal Structure of Rabbit Cytosolic Serine Hydroxymethyltransferase at 2.8 Å Resolution: Mechanistic Implications. Biochemistry, 1999. **38**(26): p. 8347-8358.

73. Schirch, D., et al., Function of the active-site lysine in Escherichia coli serine hydroxymethyltransferase. J Biol Chem, 1993. **268**(31): p. 23132-8.

จุฬาลงกรณ์มหาวิทยาลัย
Chulalongkorn University

74. Schirch, V. and D.M.E. Szebenyi, Serine hydroxymethyltransferase revisited. Current Opinion in Chemical Biology, 2005. **9**(5): p. 482-487.

75. Trivedi, V., et al., Crystal structure of binary and ternary complexes of serine hydroxymethyltransferase from Bacillus stearothermophilus: insights into the catalytic mechanism. J Biol Chem, 2002. **277**(19): p. 17161-9.

76. Contestabile, R., et al., l-Threonine aldolase, serine hydroxymethyltransferase and fungal alanine racemase. A subgroup of strictly related enzymes specialized for different functions. Eur J Biochem, 2001. **268**(24): p. 6508-25.

77. García-Cañaveras, J.C., et al., SHMT inhibition is effective and synergizes with methotrexate in T-cell acute lymphoblastic leukemia. Leukemia, 2021. **35**(2): p. 377-388.

78. Pinthong, C., et al., Distinct biochemical properties of human serine hydroxymethyltransferase compared with the Plasmodium enzyme: implications for selective inhibition. The FEBS Journal, 2014. **281**(11): p. 2570-2583.

79. Tramonti, A., et al., Human Cytosolic and Mitochondrial Serine Hydroxymethyltransferase Isoforms in Comparison: Full Kinetic Characterization and Substrate Inhibition Properties. Biochemistry, 2018. **57**(51): p. 6984-6996.

80. Gutierrez, M.L., et al., Serine hydroxymethyl transferase from Streptococcus thermophilus and L-threonine aldolase from Escherichia coli as stereocomplementary biocatalysts for the synthesis of beta-hydroxy-alpha,omega-diamino acid derivatives. Chemistry, 2008. **14**(15): p. 4647-56.

81. Kreuzman, A.J., et al., Enzymatic synthesis of diastereospecific carbacephem intermediates using serine hydroxymethyltransferase. J Ind Microbiol Biotechnol, 1997. **19**(5-6): p. 369-77.

จุฬาลงกรณ์มหาวิทยาลัย
Chulalongkorn University

จุฬาลงกรณ์มหาวิทยาลัย
Chulalongkorn University

VITA

NAME	Peerapong Wongpituk
DATE OF BIRTH	03 February 1997
PLACE OF BIRTH	Sisaket
INSTITUTIONS ATTENDED	Chulalongkorn university
HOME ADDRESS	45 M.16 Sumrongplub Pribung Sisaket 33180

จุฬาลงกรณ์มหาวิทยาลัย
Chulalongkorn University

จุฬาลงกรณ์มหาวิทยาลัย
Chulalongkorn University